Coupled CFD Framework with Mesoscale Urban Climate Model: Application to Microscale Urban Flows with Weak Synoptic Forcing

Pasha Piroozmand[a,b,*], Gianluca Mussetti[b,c,d], Jonas Allegrini[b], Mohammad Haji Mohammadi[e], Ehsan Akrami[f], Jan Carmeliet[d]

[a] Institute of Fluid Dynamics, ETH Zürich, Sonneggstrasse 3, 8092 Zürich, Switzerland
[b] Laboratory for Multiscale Studies in Building Physics, Swiss Federal Laboratories for Materials Science and Technology (Empa), Dübendorf, Switzerland
[c] Laboratory f Air Pollution /Environmental Technology, Dübendorf, Switzerland
[d] Chair of Building Physics, Swiss Federal Institute of Technology ETHZ, Zurich, Switzerland
[e] School of Engineering, University of British Columbia Okanagan, Kelowna, Canada
[f] School of Mechanical and Manufacturing Engineering, Dublin City University, Ireland

Abstract

A computational fluid dynamics (CFD) model was developed in the open-source CFD toolbox OpenFOAM for studying microscale urban flows during periods of weak synoptic forcing. The OpenFOAM model is coupled to the regional atmospheric model COSMO to provide boundary conditions for atmospheric variables. The urban canopy model DCEP is used to calculate surface energy balance and estimate the surface temperature boundary conditions. The proposed coupled model was tested for simulations of urban flows in a dense urban area of Zurich, Switzerland during a heatwave day and a day with strong background regional winds. It is shown that the coupled OpenFOAM model can qualitatively resolve small scale unsteady buoyant flows induced by heated buildings and water bodies. Comparing with the observation measurement, the coupled OpenFOAM model and COSMO can predict diurnal temperature with small errors for both sample days. For the wind speed and the wind direction, the errors of both models are higher on the heatwave day, due to the presence of unsteady buoyant flows. It is concluded that to obtain quantitatively accurate results, several improvements in transport models, surface fluxes, coupling strategies, etc. are needed. In addition, the results should be compared comprehensively with a well-located network of sensors.

1- Introduction

In the recent decades, CFD microscale models have been extensively used to study urban flows, the urban microclimate, and urban boundary layers (Toparlar et al., 2017; Mochida et al., 2011) [1, 2]. The main advantage of using CFD microscale models in comparison with regional and mesoscale atmospheric models (e.g. WRF (Skamarock et al., 2005) [3] or COSMO (Rockel et al., 2008) [4]) is their capability to accurately resolve the urban roughness sublayer (RSL), the atmospheric layer from the ground up to two-five times the mean building height, and the urban canopy layer (UCL), the atmospheric layer from the ground to the average building height, at which most of the urban environment systems and intense human activates are situated (Oke et al., 2017) [5].

CFD microscale models mostly use finite volume methods (FVM) to solve the transport equations in the scale of meters around complex urban structures such as buildings and the obstacles within an urban area. The regional and mesoscale models mostly use the finite difference method (FDM) with terrain-following coordinate systems, which are not capable of resolving geometrically urban heterogeneous structures such as sharp tall buildings. Rather, the effect of buildings on the atmosphere at the urban canopy scale is parameterized based on a statistical approach and the effects are added as source or sink terms to

* Corresponding author
E-mail address: ppasha@ethz.ch

the transport equations. In addition, the spatial resolution of the regional and mesoscale models is at most one-quarter kilometer horizontally and five meters vertically; since the embedded physical models are based on some assumptions such as horizontal homogeneity, which are not valid for higher resolutions (Schättler et al., 2008) [6]. It should be mentioned that recently applications with Immersed Boundary Methods (IBM) have been proposed to address some of the mentioned drawbacks, however, they are still at the development stage (e.g. Lundquist et al., 2010) [7].

Therefore, many important questions, such as the formation of local hot spots of the air temperature, the mechanisms of pollutant dispersion and the thermal comfort within real urban environments, can only be answered accurately by microscale CFD simulations. An interesting application of microscale CFD models is to study urban microclimate and local heat islands responses to synoptic-scale heatwaves. Heatwaves are defined as a sustained period of excessively hot days, during which the temperature is significantly higher than the average climatological mean (Li et al., 2013) [8]. Heatwaves can reduce the thermal comfort of the inhabitants of urban areas (Taleghani et al., 2015) [9], leading to health problems and, in extreme cases, even to deaths. Microscale CFD models can be a useful tool for urban planners to provide mitigation measures for such damages, however, there are several challenges in modeling the urban microclimate and urban flows with microscale models, some of which are addressed in this paper.

One of the main challenges is how to define boundary conditions for atmospheric variables at the lateral boundaries of the computational domain. Heatwaves are associated with low wind speeds due to the persistent high-pressure anticyclones (Li et al., 2013) [8]. On the other hand, high surface temperatures induce buoyant forces. Due to high temperatures and low wind speeds, the order of magnitude of thermal buoyancy forces and buoyant production of turbulence can be comparable in size to mechanical shear forces and shear turbulence production, respectively. This interaction within a highly heterogeneous urban environment leads to complex spatially and temporally varying vertical profiles of atmospheric variables. Therefore, the traditional approach of specifying lateral boundary conditions with fixed direction logarithmic surface layer profiles cannot be applied (Mochida et al., 2011, Li et al., 2017) [2, 10]. These logarithmic profiles assume a stationary and horizontally homogeneous atmospheric boundary layer (ABL) with constant vertical shear flux at the surface layer, which is not the case for heatwave events (Richards and Norris, 2011) [11]. Using generalized logarithmic profiles based on MOST (Monin-Obukhov Similarity Theory), e.g. Temel and van Beeck, 2017 [12], may also not be applicable, since the stationary and horizontal homogeneity assumption is still assumed to hold true. To address this challenge, we use a regional mesoscale atmospheric model, COSMO, by which the heatwaves characteristics at a synoptic scale and the interaction with the urban heat island (UHI) can be captured, providing accurate varying (in magnitude and direction) vertical profiles of atmospheric variables with a reasonable resolution. Then, the lateral boundaries of the microscale CFD model are updated by the interpolation from vertical profiles of the atmospheric variables of the driving regional atmospheric model.

Buoyancy is another important factor that defines the state of the urban atmosphere during heatwaves. The buoyant flows are driven by hot urban surfaces, which vary temporally and spatially. Therefore, the temperature boundary condition of urban surfaces is needed to accurately model the microscale urban flows. Knowing the temperature at each point of urban element surfaces, e.g. roofs, walls, streets and water bodies, would be difficult to achieve, since the surface temperature is a function of short and long wave radiative energy exchanges, sensible and latent heat flux between the surface and the air, and conduction through the materials (Schrijvers et al., 2015; Liu et al., 2012) [13, 14]. A time-dependent surface energy balance (SEB) equation needs to be solved at each point, which highly depends on 3-D configuration of urban elements and the material and surface characteristics (Oke et al., 2017) [5].

Kubilay et al. (2018) [15] proposed an integrated microclimate model in OpenFOAM (Jasak et al., 2007) [16], which solves the heat and moisture transports in materials, and radiative heat transfer at the surface using radiosity approach. This method works well for the street canyon scale but is computationally demanding for larger scales. Studying local hot spots, Allegrini and Carmeliet (2018) [17] performed building energy simulations (BES) to provide temperature boundary conditions for the CFD analysis, which required BES setup and was limited to one-way coupling. Both methods also rely on uncertain prior input information about the surface and material characteristics. Focusing more on the simulation of airflows, there exist more simplistic approaches to estimate surface heat fluxes. Liu et al. (2012) [14] used a simple

energy balance equation, in which the radiation part is empirically calculated and therefore the temperature at each face point is calculated merely by knowing the adjacent air temperature and the material temperature. Gao et al. (2018) [18] used infrared images from observations and the time-dependent surface temperatures were prescribed by image processing and interpolation techniques. Vonlanthen et al. (2017) [19] used constant surface temperatures for buildings and the ground in their LES study of the convective ABL over a realistic terrain. Kwak et al. (2015) [20] interpolated WRF near-surface temperatures to specify the ground temperatures and assumed adiabatic building walls. Recently, the urban microscale model PALM-4U has been developed, which resolves the airflow and transport of other species within urban environments using LES models, while it also directly calculates the surface energy balance at the building scales (Maronga et al.) [21].

If one wants to focus on urban flows in UCL or RSL layers during weak synoptic forcing conditions, the mentioned methods can either be unnecessarily computationally demanding or too simplistic and inaccurate. As a computationally efficient estimation of the time-dependent surface temperature of buildings and on the ground, we use the building effect parametrization (BEP) scheme embedded in COSMO (Martilli et al., 2002) [22]. Double Canyon Effect Parametrization (DCEP) is a BEP model in COSMO, whose task is to calculate SEB at urban elements (Schubert et al., 2012) [23]. DCEP provides the surface temperatures of roofs, walls, and streets at a horizontal spatial resolution of the mesoscale model, but with meter-scale vertical spatial resolution, from which heat fluxes are calculated and eventually integrated as volumetric source or sink terms into COSMO cell points. Here, we directly extract the surface temperatures calculated in DCEP and then interpolate them in the CFD microscale model to provide the surface temperature boundary conditions. In general, OpenFOAM is coupled separately to COSMO and DCEP for lateral and surface boundary conditions, respectively. COSMO and DCEP are two-way coupled themselves. In our approach, the coupling of COSMO and DCEP to OpenFOAM is done in a one-way approach. The two-way coupling can be implemented e.g. in a way that OpenFOAM provides velocity values for DCEP, and DCEP calculates SEB to provide temperature boundary conditions for OpenFOAM building surfaces. This approach has the potential to provide more accuracy, however, due to possible inconsistencies between the physical models and coding languages of OpenFOAM and COSMO-DCEP, this option is not tested in this paper.

The rest of the paper is organized as follows: Section 2 describes the methodology used for simulations. First, the microscale CFD model implemented in OpenFOAM is described. Then the regional atmospheric model in COSMO and the urban canopy model in DCEP are briefly explained. The coupling strategy including how to extract the initial and boundary conditions from COSMO and DCEP for OpenFOAM is explained. In Section 3, a case study is defined for a dense urban area in the city of Zurich in Switzerland. Further, the numerical setup and models configurations are described. In Section 4, first, the capabilities of the coupled model are highlighted. Then, for two days the results of the performed simulations are compared with field observations: one day before a heatwave event with strong background regional winds and one day at the peak of the heatwave. A quantitative assessment of OpenFOAM and COSMO simulations based on different error norms is also presented in this section. Finally, Section 5 presents conclusions on the performance of the proposed method and provides comments on the limitations of the new approach and discusses possible future works.

2- Methodology

2-1- The CFD model

The system of Reynolds Averaged equations, governing mean transport of mass, momentum and energy, referred to as Unsteady Reynolds Averaged Navier-Stokes (URANS) equations, reads

$$\frac{\partial U_i}{\partial x_i} = 0, \tag{1}$$

$$\frac{DU_i}{Dt} = \frac{\partial}{\partial x_j}\left(\nu\frac{\partial U_i}{\partial x_j} - \tau_{ij}\right) - \frac{\partial p}{\partial x_i} - \beta g_i(\theta - \theta_{ref}) \text{ and} \quad (2)$$

$$\frac{D\theta}{Dt} = \frac{\partial}{\partial x_i}\left(\frac{\nu}{Pr}\frac{\partial \theta}{\partial x_j} - \tau_{\theta j}\right), \quad (3)$$

where $\vec{U}$ and θ are the mean velocity and the potential temperature, τ_{ij} and $\tau_{\theta j}$ are the Reynolds stress and the turbulent heat flux components, respectively, and p is the pressure. Further, ν, Pr, β and θ_{ref} are the kinematic viscosity, Prandtl number, thermal expansion coefficient and reference potential temperature, respectively. The flow is assumed to be incompressible, and the Boussinesq approximation for the buoyancy force is applied. These assumptions are justified, since studying the stratification of urban boundary layers (UBL) is not the focus here. Moreover, since the urban atmosphere in the UCL and RSL is the focus of this paper, the Coriolis force is neglected. The components τ_{ij} and $\tau_{\theta j}$ are computed assuming linear eddy-viscosity and simple gradient diffusion hypotheses (SGDH), i.e.,

$$\tau_{ij} = \frac{2}{3}k\,\delta_{ij} - \nu_t\left(\frac{\partial U_i}{\partial x_j} + \frac{\partial U_j}{\partial x_i}\right) \text{ and} \quad (4)$$

$$\tau_{\theta j} = -\frac{\nu_t}{\sigma_\theta}\frac{\partial \theta}{\partial x_j}, \quad (5)$$

where k is the turbulent kinetic energy (TKE) and σ_θ is the turbulent Prandtl number. The turbulent viscosity ν_t is calculated as

$$\nu_t = C_\mu\frac{k^2}{\varepsilon}. \quad (6)$$

Using standard K-epsilon turbulence model, to compute the TKE (k) and its dissipation rate (ε) the two transport equations

$$\frac{Dk}{Dt} = \frac{\partial}{\partial x_j}\left(\frac{\nu_t}{\sigma_k}\frac{\partial k}{\partial x_j}\right) + P + G - \varepsilon \text{ and} \quad (7)$$

$$\frac{D\varepsilon}{Dt} = \frac{\partial}{\partial x_j}\left(\frac{\nu_t}{\sigma_\varepsilon}\frac{\partial \varepsilon}{\partial x_j}\right) + \frac{\varepsilon}{k}[C_{\varepsilon 1}(P + C_{\varepsilon 3}G) - C_{\varepsilon 2}\varepsilon] \quad (8)$$

are solved, where *P* is the mechanical turbulence production term and *G* is the buoyant turbulence generation/destruction term. The term *G* is not defined in the standard turbulence models for incompressible flows and is not found in OpenFOAM's libraries. We model the term *G*, which is crucial for modeling buoyant flows, as

$$G = \beta g_i \tau_{\theta j}. \quad (9)$$

It is well known that the standard K-epsilon model, which is based on linear eddy-viscosity assumption, show difficulty in resolving complex 3-D flows such as urban flows, where strong pressure gradient, separation regions and streamline curvature exist (Longo et al., 2017) [24]. In addition, the model in conjunction with SGDH assumption of turbulent heat flux cannot properly deal with the buoyancy effect on the velocity and temperature fields. Nonetheless, since the focus of this study is more to demonstrate the coupling approach and also since this model has been used and well documented by the community, we opted to use this model. The model has to be validated with well-designed experiments in water tanks or water tunnels using time-resolved PIV-LIF data for velocity and temperature.

The turbulence model constants C_μ, σ_k, σ_ε, $C_{\varepsilon 1}$, $C_{\varepsilon 2}$ and $C_{\varepsilon 3}$ are the standard K-epsilon coefficients and their values are listed in Table 1. It should be mentioned that in the convective boundary layer over an urban complex terrain parameters such as σ_θ or C_μ are not constants and would be highly variable in space. However, it has been shown that any attempt to tune the parameter values for one location may result in huge errors in other locations (Temel et al., 2018) [25]. In addition, as Richards and Norris (2019) noted, attempts to force a consistency between these parameters of turbulence equations and an appropriate atmospheric boundary layer profile may lead to inconsistency with the momentum equations (Richards and Norris, 2019) [26]. Since in our study the regions of interest lie within the RSL and UCL, we keep the constant default values, which are more suitable for near-surface regions.

Table 1- Values for coefficients of the standard K-epsilon turbulence model [27]

C_μ	σ_k	σ_ε	$C_{\varepsilon 1}$	$C_{\varepsilon 2}$	$C_{\varepsilon 3}$	σ_θ	κ
0.09	1.0	1.3	1.44	1.92	$\tanh\left\lvert\frac{U_{ver}}{U_{hor}}\right\rvert$	0.9	0.41

2-2- COSMO-DCEP

2-2-1- COSMO

COSMO is a non-hydrostatic limited-area regional atmospheric model based on primitive thermo-hydro-dynamical equations, which describe compressible flow in a moist atmosphere (Schättler et al., 2008) [6]. It is formulated for generalized terrains following the height coordinate. Different physical processes such as precipitation, cloud cover, surface fluxes, and soil processes are parameterized. The model equations are numerically solved using finite difference schemes. For further information, the readers are referred to Refs. [4, 6, 28, 29] (Rockel et al., 2008; Schättler et al., 2008; Doms et al., 2011a; Doms et al., 2011b).

2-2-2- DCEP

DCEP is a multi-layer BEP scheme embedded in COSMO, which represents the dynamical and thermal impact of buildings on airflow. Being seen as a black box, DCEP receives inputs including velocity, TKE, and temperature from COSMO cells, computes the effect of the urban surfaces on the airflow (e.g. drag, heat flux and turbulence production induced by buildings). As output, it provides source or sink terms for the transport equations solved by COSMO.

As it is shown in Fig. 1(A), DCEP uses a different structured computational grid than COSMO. DCEP column of layers horizontally matches the horizontal coordinates and the size of COSMO cells but their z coordinates are different from z coordinates of COSMO grid cells. DCEP column of layers typically consists of 13 layers, each layer with a height of around 5-20 m. The height of the column of layers can be around 120 m, which roughly corresponds to 6-7 COSMO grid cells. Since the z coordinates of COSMO and DCEP grid cells do not overlap, the two-way exchange of information between COSMO and DCEP cells requires interpolation and integration.

The main feature of DCEP model is that, instead of an actual geometrical representation of an urban canopy, it is conceptualized into quasi-two-dimensional street canyons for four distinct orientations: North-South, Northeast-Southwest, East-West, and Northwest-Southeast (Fig. 1(B)). The total building effect on COSMO cells as sink or source terms is calculated by summing up the values of each orientation weighted on the fraction of street canyon orientations (FR_{UDir}). At each orientation, the urban canopy comprises identical neighboring street canyons each of which are characterized with one road, one row of building, and two walls (Schubert et al., 2013) [30]. Since the street canyons are assumed to be identical, the calculations are done for one street canyon, and the values, e.g. the calculated flux from the urban canopy to the airflow, are multiplied by the number of similar street canyons that fill the COSMO grid cell (e.g. multiplied by 10, if the width of the street canyon element is 25 m and the width of the COSMO cell is 250 m). Three main parameters define geometrical characteristics of the street canyon: W and B are the street and building width, and γ_i is the fraction of buildings (the ratio of the volume of buildings elements to the total volume of the layer) in the vertical layer i (Fig. 1(C)).

To calculate the heat source or sink terms in COSMO cells, DCEP calculates the temperature or heat flux at the surface of the roof, the walls and the street. The material (e.g. the concrete for walls and roofs, and the soil for the street) is discretized in one dimensional volumetric layers, and then a non-stationary heat diffusion equation is solved, assuming temporally constant temperature at the inner part of materials (the grid at the interior of materials is not shown in Fig. 1(C)). Then, the SEB equation is solved at the interface of materials and the air, which includes the energy budget of shortwave and longwave exchanging radiations, the sensible heat flux and calculated conductive heat flux from the materials. The solution of the SEB equation at each time step provides a time-dependent surface temperature or heat flux, and they can be integrated over DCEP column of layers and weighted averaged on FR_{UDir} to provide heat source and sink terms in COSMO cells. For further information, the readers are referred to Refs [22, 23, 30] (Martilli et al., 2002; Schubert et al., 2012; Schubert, 2013).

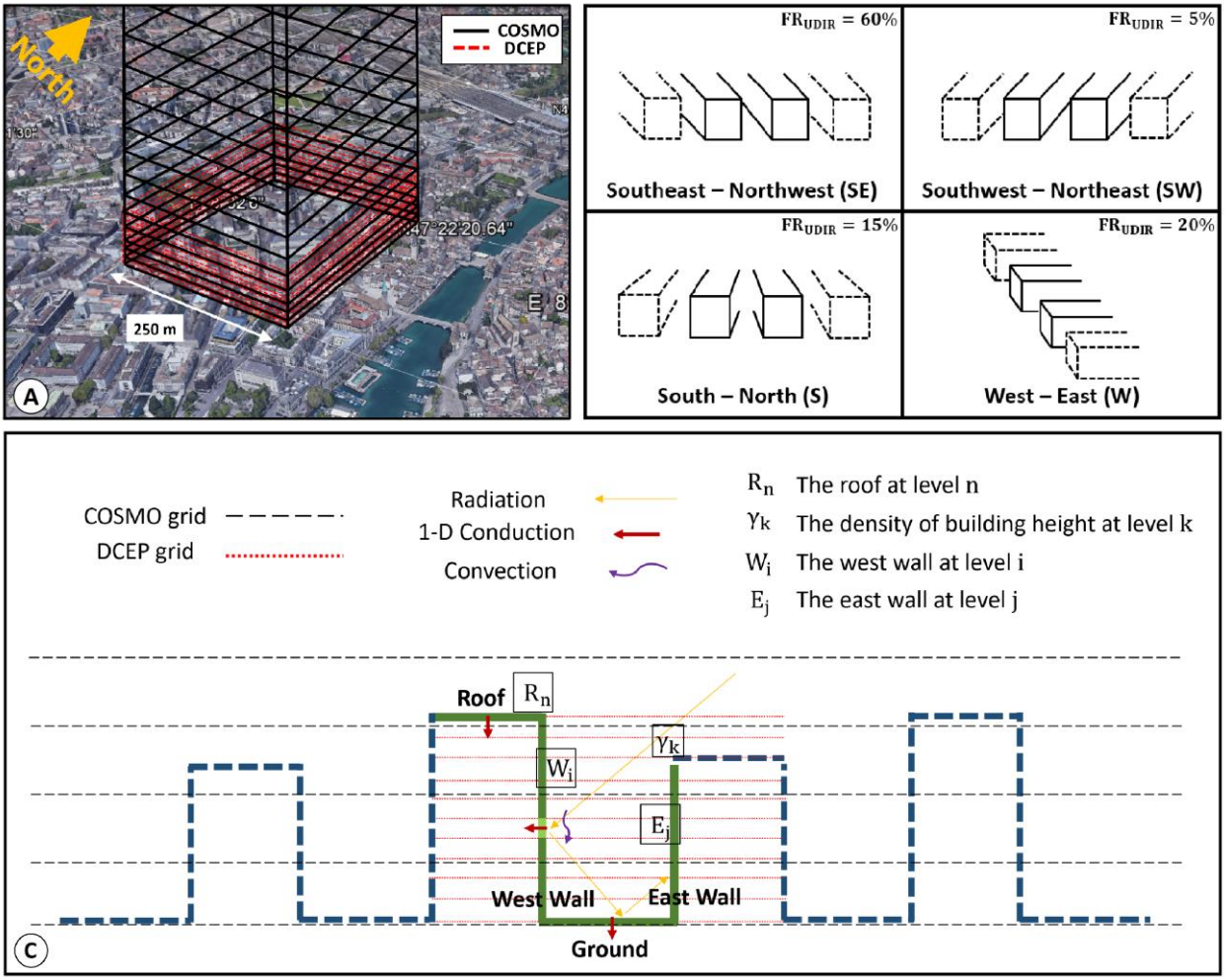

Fig. 1. The DCEP urban canopy model. (A) The grid cells of DCEP and COSMO. To better illustrate the difference of COSMO and DCEP grid cells, the heights of cells are depicted with exaggeration in the z-direction (adapted from Google Earth). (B) An example of compiling an urban canopy to four representative street canyons with different orientations weighted on the urban fraction of orientations (FR_{UDIR}). (C) DCEP computational street canyon element. Regardless of the street orientation, the left-hand side wall is called the west wall and the right-hand side wall is called the east wall (adapted from Schubert, 2013 [30]).

2-3- Coupling strategy

2-3-1- Initial Condition

To generate the initial condition for the coupled CFD microscale model developed in OpenFOAM (for simplicity, from now on, it is called OpenFOAM), COSMO coarse results for velocity ($\vec{U}$) and TKE (k) are interpolated via a 3-D Moving Least Square (MLS) method with tri-linear basis functions. The MLS is an approximation method to reconstruct continuous functions from a number of random sample points (here adjacent COSMO cells). MLS calculates a weighted least squares (WLS) measure biased towards the surrounding region of the location of interest (here the value at the OpenFOAM cell center) (Haji Mohammadi et al., 2014) [31].

The turbulent dissipation rate (ε) is initialized via the following relation, which is based on the equilibrium assumption and the linear relation between the turbulent length scale versus height from the ground (z):

$$\varepsilon_{initial} = \frac{C_\mu^{\frac{3}{4}} k^{\frac{3}{2}}}{\kappa z}. \tag{10}$$

The internal potential temperature (θ) is assumed time-dependent and spatially uniform. The constant potential temperature is assigned from averaging over the COSMO inertial sublayer (ISL) cells, corresponding to 4-6 vertical cell levels. Directly interpolating COSMO temperature in OpenFOAM would lead to numerical errors and divergence due to the inconsistency between the thermodynamic COSMO and OpenFOAM models (Tewari et al., 2010) [32]. The error of the assumption of vertical uniformity would not be significant: if one focuses on the RSL and UCL (this study focuses on the effect of temperature differences via buoyancy on the urban flow rather than on the vertical temperature profile itself) and if the daytime (the hottest period of the heatwave day, e.g. around noon) is the main time period of the study since during that period the vertical UBL profile of the potential temperature over RSL is almost constant (Oke et al., 2017) [5].

2-3-2- Lateral and top boundary conditions

Similar to the previous section, unsteady velocity and TKE at all lateral and top boundaries are directly interpolated from COSMO via the MLS method and imposed as Dirichlet boundary conditions. At OpenFOAM time steps, which are between two consecutive COSMO time step intervals, values are linearly interpolated in time. Constant vertical profiles of the potential temperature at lateral and top boundaries are updated each time step similarly as described in the previous section. Zero gradients are assumed for the turbulent dissipation rate and the pressure.

Since the system of equations and computational grid resolutions are different in COSMO and in the OpenFOAM models, mass conservation may not be satisfied and can lead to immediate divergence of the solution. Therefore, similar to the application by Rodrigues et al. (2016) [33], mass conservation is enforced by multiplying a correction factor to the velocity value of the OpenFOAM boundary cells at each lateral and top boundary surface using the relation

$$\varphi_i = 1 - \mathrm{sgn}(\dot{m}_\iota) \frac{\sum_j \dot{m}_j}{\sum_j |\dot{m}_j|}, \tag{11}$$

where $\dot{m}_\iota$ is the mass flux at a lateral or the top boundary surface.

Due to different spatial resolutions and the use of different sets of equations in COSMO and OpenFOAM, numerical noise caused by the mismatches may propagate from boundaries into the internal zone of the OpenFOAM model. A blending layer is employed at the lateral and top boundaries of the OpenFOAM model in order to reduce the errors caused by such mismatches (Doms et al., 2011a) [28]. Towards lateral and top boundaries, the blending layer mixes prognostic variables calculated by OpenFOAM with those calculated by COSMO via implicit sourcing with a suitable relaxation time. For the velocity, TKE and the potential temperature a source/sink term is added to the right-hand side of the equations [33], i.e.,

$$\frac{D\phi_{OF}}{Dt} + f(\phi_{OF}, x) = \frac{1}{\tau_r}(\phi_{COSMO} - \phi_{OF}) \sin^2\left(\frac{\pi}{2}\frac{L-l}{L}\right), \qquad l < L, \tag{12}$$

where ϕ is the prognostic variable in OpenFOAM or COSMO. The left-hand side is the generic transport equation, L is the thickness of the blending layer, l is the distance of the grid cell to the boundary and τ_r is the relaxation time, which specifies the blending strength.

2-3-3- Surface boundary condition

For wall-adjacent cells, equilibrium wall functions are implemented (Blocken et al., 2007) [34]. This assumption might introduce some errors due to the existence of the buoyancy force, pressure gradient, etc. in our coarse wall cells, which are far larger than centimeter logarithmic regions. There are some developments for taking into account the non-equilibrium effect but they are not yet well established and widely used (Popovac and Hanjalic, 2007, Allegrini et al., 2012) [35, 36].

No-slip boundary conditions are assumed for the velocity. The wall shear stress is calculated by assuming the log-law profile for fully rough walls and is imposed by modification of the turbulent viscosity at the wall. TKE is updated by adding mechanical TKE production (P) in the wall-adjacent cells neglecting the non-equilibrium terms. The turbulent dissipation rate is then computed from the local equilibrium assumption ($P = \varepsilon$). For the temperature, based on the local equilibrium assumption, the kinematic wall heat flux is introduced to the energy equation by modification of the turbulent thermal diffusivity at walls multiplied by the surface temperature gradient. However, to calculate the surface temperature gradient ($(\theta_P - \theta_{surf})/Z_{cell}$), the surface temperature is needed.

As it is described in section 2-2-2, DCEP can predict street temperatures (weighted average on $\mathrm{FR_{UDIR}}$) with a horizontal spatial resolution of $250\ \mathrm{m} \times 250\ \mathrm{m}$. The time-dependent temperature boundary condition for the ground surfaces in OpenFOAM is then assigned by interpolation of four adjacent DCEP ground temperatures using a 2-D MLS method. DCEP also calculates the temperatures of roofs at 13 height levels (from 5 m to 100 m). Similar to the ground temperatures, the temperatures of OpenFOAM roof boundaries are calculated by performing 3-D MLS interpolations (weighted average on $\mathrm{FR_{UDIR}}$). For walls, DCEP calculates temperatures in a similar way as for roofs, i.e., at 12 height levels (from 2.5 m to 90 m). Since each street canyon has west and east walls, having 4 street canyon orientations, there are totally eight wall temperature values at each 12 height levels. The temperature of a cell face at a building wall in OpenFOAM is computed from the corresponding DCEP wall temperature values using the 3-D MLS method. The algorithm for updating the surface temperature boundary condition can be summarized as follow:

1. Sweep over OpenFOAM surface faces of surface adjacent cells, to update their temperatures.
2. At each cell face, determine the type of the surface on which the cell face exists: the roof or the wall or the ground.
3. If it is a wall face, find the surface orientation from eight possibilities. For example, if the wall normal vector in OpenFOAM is oriented to the north-east, then corresponding DCEP orientation is the west wall of the street canyon oriented from south-east towards the north-west ($\mathrm{Wall_{SE_W}}$).
4. Find four DCEP columns of layers which are closest to the horizontal location of the face cell.
5. Having the height of the cell face from the ground in OpenFOAM, find two layers of DCEP where the cell face height is between the height of those DCEP layers.
6. From steps 4 and 5 we can find 8 DCEP cells which construct a hypothetical hexahedron which the OpenFOAM cell face is located within the hexahedron volume.
7. Using Moving Least Square method, interpolate the value of the temperature at the cell face from 8 values of adjacent corresponding DCEP cells (eight $\mathrm{T_{Wall_{SE_W}}}$ in DCEP estimates the OpenFOAM cell face temperature located on a north-east oriented wall).

We skip steps 3 and 6 for the roof since defining a physical orientation for a roof is difficult. Instead, the OpenFOAM roof temperature is estimated by eight corresponding DCEP values weight averaged on FR_{UDIR}. For the ground, only steps 1, 2, 4, and 7 are needed and similar to the procedure for the roof, the ground value is estimated by four corresponding DCEP values weight averaged on FR_{UDIR}.

As an instance to illustrate the algorithm, the temperature at an OpenFOAM cell face, which is located on the southwest-oriented wall of a building with its face center at 6 m above ground, is interpolated from eight adjacent DCEP temperature values: four adjacent DCEP temperatures at $\mathrm{Wall}_{\mathrm{NE_W}}$ (the west wall of the Northeast-Southwest street direction) on the first vertical layer (at 2.5 m) and four adjacent DCEP temperatures at $\mathrm{Wall}_{\mathrm{NE_W}}$ on the second vertical layer (at 7.5 m). This can provide some accuracy to the model. For example, at noon a wall oriented to the south has a higher temperature than a wall oriented to the north since the former can be exposed to the sun short-wave radiation. An example of implementing this procedure within the urban area is depicted in Fig. 2(B-C). The general procedure of the coupling is summarized and illustrated in Fig. 3.

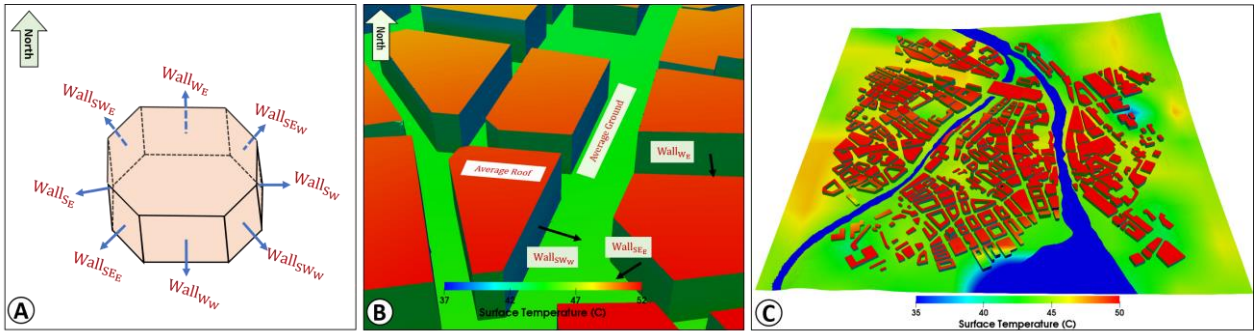

Fig. 2. The surface temperature boundary condition at roofs, wall, and the ground in OpenFOAM interpolated from DCEP. (A) The walls of the OpenFOAM geometrical model are grouped into eight orientations. E.g. $\mathrm{Wall}_{\mathrm{NW_E}}$ corresponds to a building wall with northwest-southeast direction. (B) An example of the specification of the surface temperatures within the urban area using DCEP results. (C) The MLS method provides a realistic surface temperature distribution in the whole domain.

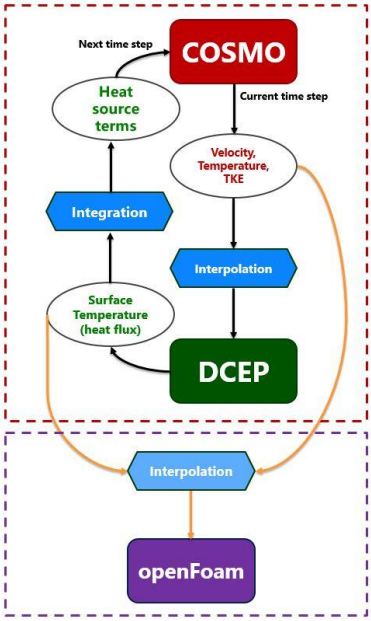

Fig. 3. The general procedure of the coupling approach. The two-way coupling between COSMO and DCEP and one-way coupling between COSMO-DCEP and OpenFOAM. The right yellow arrow shows the use of COSMO's atmospheric variables to update the initial and lateral and top boundary conditions. The left yellow arrow indicates the use of computed surface temperatures from DCEP in OpenFOAM to set temperature surface boundary conditions.

3- Case Study

The coupling approach is tested for simulations of urban flows in a dense urban area in Zurich, Switzerland. Zurich is located in north-central Switzerland at the north-western tip of Lake Zurich. The horizontal size of the computational domain is 2.5 km × 2.5 km and its height is about 1 km above sea level and around 600 m above the ground (Fig. 4). The topology and geometrical building models are from Ref. [37]. The building geometries are at the "level of detail of 1 (LoD1)". In LoD1 city models, buildings are represented as prismatic blocks with flat roof structures (Gröger et. al, 2008) [38]. Building geometries are further corrected and simplified e.g. removing errors such as non-manifold edges, increasing the minimum geometrical feature to 10 m, filleting a few sharp edges (less than 30^{o}) where highly skewed meshes may be generated, etc.

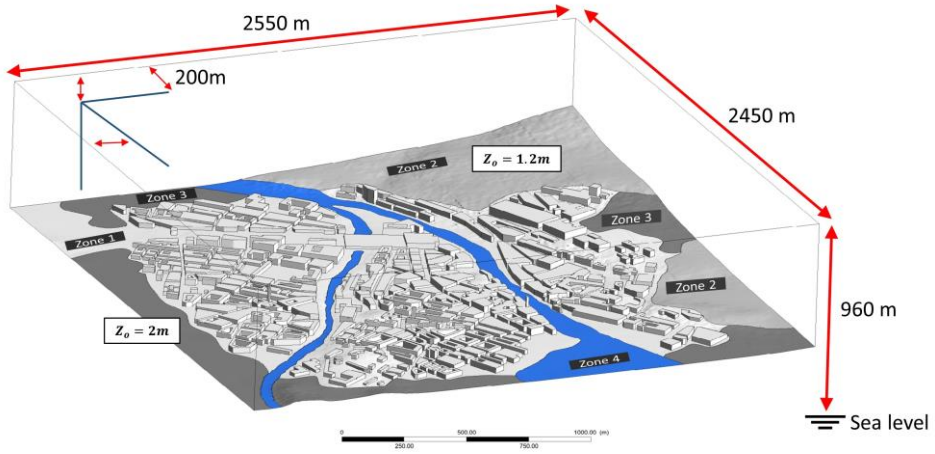

Fig. 4. The geometrical model and the computational domain of the microscale CFD model.

According to Fig. 4, the ground surface is divided into four distinct zones. The geometrically-resolved zone at the center of the domain, in which buildings are geometrically modeled (zone 1 in Fig. 4). In this zone, the equivalent sand-grain roughness at the ground surface and buildings are assumed to be 0.005 m. The northeast and a part of the eastern regions of the urban area in the domain, where small residential buildings with similar heights are located in a statistically uniform way, is modeled as a rough wall with an aerodynamic roughness length of 1.2 m (zone 2 in Fig. 4). In the remaining border zones, up to about 250 m away from the domain boundaries, tall buildings are not resolved; instead, that urban area is modeled as a rough wall with an aerodynamic roughness length of 2 m (zone 3 in Fig. 4). This crude modeling may cause some inaccuracies at the incident flows. Nonetheless, it is necessary since, geometrically modeling of buildings close to lateral boundaries may cause numerical errors, due to the mismatches between the OpenFOAM computation and the blending layer effect. All unsteady lateral and top boundaries are updated by COSMO results and the surface temperatures are prescribed from DCEP results. For rivers and the lake surface temperature (zone 4 in Fig. 4), a uniform but time-dependent temperature value is chosen from the COSMO cell located in the lake but close to the river.

Two CFD simulations cover two case days, one just before and one at the peak of a heatwave event. The first simulation period starts at 1800 UTC on June 22, 2015 and finishes at 0000 UTC on June 24, 2015.

This case corresponds to a typical summer day of June or July in Zurich, with strong background regional winds. The second simulation period covers 1200 UTC on July 1, 2015 till 0000 UTC on July 3, 2015. July 2, 2015 is a calm and sunny heatwave day with high temperatures and low wind speeds. For the normal summer day, the first 6 hours are discarded as spin-up and for the heatwave day the first 12 hours. This results in 24 hours of simulations for further analysis. The spin-up times may be seen a bit short and if one seeks to completely eliminate the initial condition effect one needs to run the model at least couple of days before starting the analysis, which is computationally very expensive (Koblitz et al., 2015) [39]. However, since we initialize the OpenFOAM simulation with COSMO values, which are realistic and already consistent with the boundary conditions imposed by COSMO, the spin-up time may not be necessarily too long. The only region which deviates from the initial values substantially is the UCL and RSL, where the time and length scales are small enough to be adapted in a couple of hours. In addition, by rough estimation, it can be shown the flow would pass the domain at least ten times, if we assume 6 hours for strong winds on June 23 and 12 hours for weak winds on July 2.

The computational grid was generated with snappyHexMesh, which is the standard mesh generation tool in OpenFOAM. The mesh contains 4.6 million cells with cell sizes of 1-32 m. To verify the mesh independence, a finer mesh with one more level of refinement and 17 million cells (cell size of 0.5 m – 32 m) was generated. Based on Fig. 5(A), the transient temperatures at Kaserne station computed by the model using two meshes follow the same trend with small differences, especially in comparison with the simulation error with respect to the observation. Vertical profiles of hourly average wind speed using the fine mesh at three sample locations, i.e., at Bahnhofstrasse, Munsterhof and Kaserne (the locations are shown in Fig. 10) are compared with the corresponding vertical profiles in the chosen mesh. It was found that the averaged relative errors (from the ground up to 600 m height above sea level) associated with the chosen mesh are 0.01, 0.03, and 0.02 m/s, respectively (Fig. 5(B)).

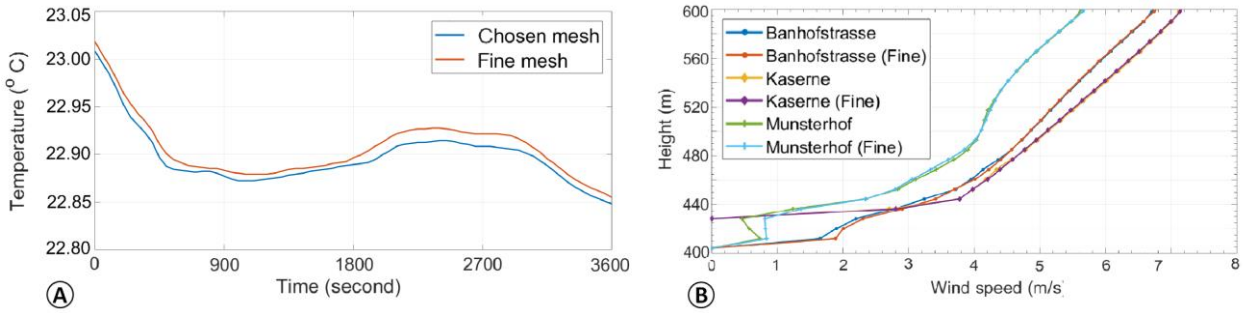

Fig. 5. Performance comparison of results for the chosen mesh and the fine mesh. (A) The 1-hour time series of the potential temperature at Kaserne weather station (the location is shown in Fig. 10) obtained with the chosen mesh and the fine mesh. (B) The hourly average wind speed versus the height above sea level at three sample locations for the chosen mesh and the fine mesh.

The contours of the hourly average temperature and wind speed distributions at 3 m above the surface also show small differences between the fine and the chosen mesh (Fig. 6). Since for a URANS study, smaller cells require smaller time steps to maintain the maximum CFL number value, the simulations with a twice fine mesh needs eight times more computational time. Therefore, considering the relatively small differences between two meshes, and considering errors and uncertainties of the model with respect to the observation, we continue with the 4.6 million cell mesh.

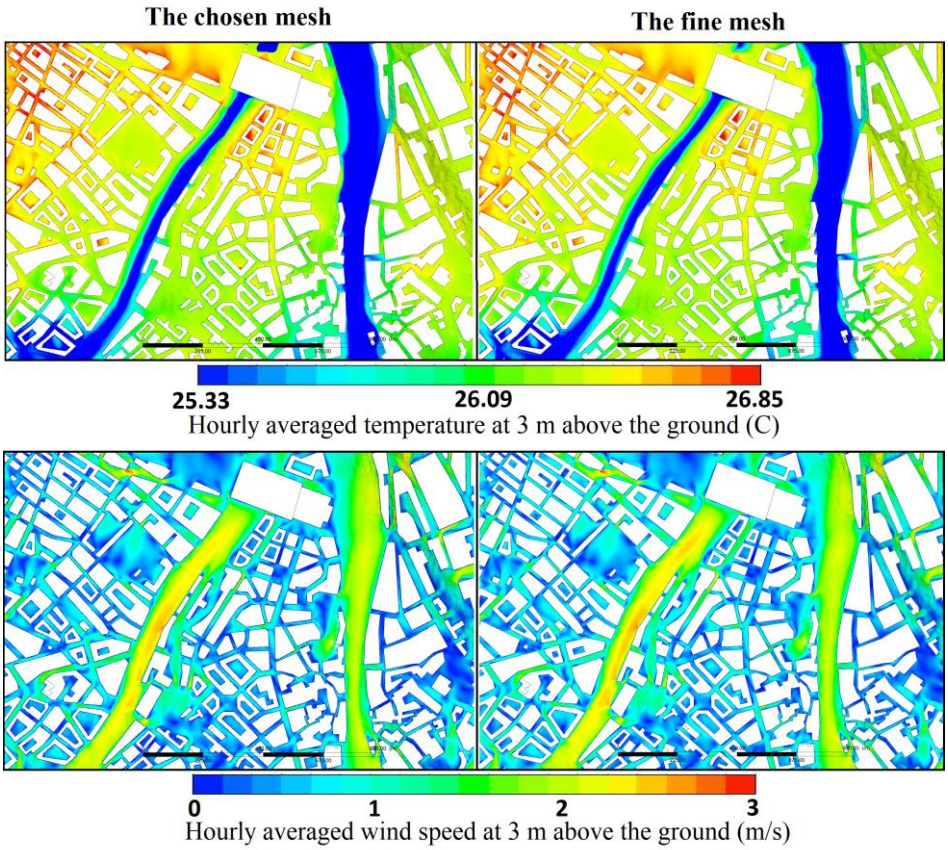

Fig. 6. Temperature and wind speed distributions at 3 m above the ground for the chosen and the fine mesh.

3-1- COSMO setup

The planetary boundary-layer scheme is based on Ref. [40] (Mellor & Yamada, 1982). The radiation scheme is based on the δ two-stream version of the radiative transfer equation (Ritter and Geleyn, 1992) [41] and shallow convection is parameterized by the Tiedkte (1989) scheme [42]. COSMO also includes a multi-layer soil model, a vegetation parameterization and a cloud microphysics scheme (Doms et al., 2011) [29]. COSMO is applied over a domain with the size of approximately $50\ \text{km} \times 50\ \text{km}$ using a horizontal grid spacing of 250 m. Mussetti et al. (2019) proved that the model has the capability to be exploited up to this spatial resolution [43]. 76 levels were used in the vertical direction, with 6 and 23 levels in the first 100 m and 1000 m, respectively. The simulations cover a time period of 18 days from 20 June 2015 to 8 July 2015. Atmospheric analyses from the operational COSMO-2 model, operated by the Federal Office of Meteorology and Climatology of Switzerland (MeteoSwiss), were used as initial and boundary conditions. The analyses cover the entire Alpine range with a spatial resolution of about 2 km. The analyses are generated from the operational forecast using a nudging technique (Schraff, 1997) applied to near-surface and vertical profile observations of pressure, relative humidity and wind [44].

3-2- DCEP setup

Specific urban canopy parameters have been derived for each COSMO grid cell in the domain using high-resolution datasets of urban fraction and building geometries. Input data such as surface fraction covered by buildings (f_{urb}), building height distribution (γ), building and street width distribution ($W_{building}$, W_{street}) are derived from a 3-D building model (Swisstopo, 2010 [45]) covering the entire domain with a level of detail of 1 (LoD1). The anthropogenic heat flux (AHF) was neglected in this study. Musseti et al. [43] showed that AHF in Zurich is roughly $20 - 40\ \text{W/m}^2$, and it has a small influence on

the energy balance. The material properties of roof (R), wall (W) and street surfaces (G) follow the proposals of Schubert et al. 2013 [30]: the corresponding emissivities are $\varepsilon_R = \varepsilon_W = 0.9$ and $\varepsilon_G = 0.95$ and the thermal diffusivities are $k_R = k_W = 0.67 \times 10^{-6}\ m^2\ s^{-1}$ and $k_G = 0.29 \times 10^{-6}\ m^2\ s^{-1}$. Furthermore, the same value of the volumetric specific heat capacity is used for all surfaces: $c_R = c_W = c_G = 2.3 \times 10^6\ J.m^{-3}.K^{-1}$. Typical albedo values for roof and street surfaces are chosen according to Loridan and Grimmond (2012): $\alpha_R = 0.15$ and $\alpha_G = \alpha_W = 0.1$ [46]. It should be mentioned that the constant values used for DCEP cells may not be very accurate as the material and surface characteristics are spatially changing within the domain. However, since the focus is on the flow rather than the surface temperature itself, the accuracy may be justified.

3-3- OpenFOAM numerical setup

The unsteady incompressible RANS equations are solved with the OpenFOAM CFD toolbox v. 1612+ using the PIMPLE algorithm. The Euler scheme is used for time discretization. The hybrid second-order discretization schemes are used for divergence terms and linear interpolation for gradient and Laplacian terms. The discretized equations are solved using preconditioned conjugate gradient solvers. 10^{-5} is set as a convergence criterion for all solutions except for the pressure, for which it was set to 10^{-4}. The time step was set to 0.2 s leading to maximum CFL numbers in the range of 2-4. The blending layer thickness is 200 m. The relaxation time τ_r in Eq. (12), was set to 0.05 (Rodrigues et. al, 2016) [33]. The values of COSMO and DCEP are saved every 30 and 15 minutes for June 23 and July 2 cases. Whenever OpenFOAM reaches the time where data of COSMO and DCEP are available it reads the values and use them for boundary conditions. On the other time steps, the values of COSMO and DCEP at two consecutive time steps are linearly interpolated in time and imposed to the OpenFOAM boundaries. Due to storage limitation, the results of OpenFOAM are saved every 50 s.

4- Results and Discussion

4-1- Qualitative assessment of the coupled approach

Before comparing the coupled approach's results with the observations, we highlight the improved spatial resolution of the coupled OpenFOAM model compared to COSMO. In addition, we show some qualitative analysis, which is possible with the proposed coupled approach. To show how temperature differences in the urban environment affect the urban flows via the buoyancy effect, in Fig. 7 the hourly averaged streamlines and air temperatures (in the X-Z plane at Y=1500 m) at 2 pm July 2 are shown. According to this figure, the heated urban surfaces add upward momentum to the wind, which blows from the east, and lead to hot spot circulation zones on the right-hand side of the river. Also, it can be seen that the river, due to the downward buoyancy force, deflects the airflow downwards and the flow carries the cold air with itself to the left-hand side of the river. The streamlines on the building on the left-hand side of the river also show the buoyant flows induced from the hot roofs. The cooling effect of the river is also manifested by the temperature contours. This qualitatively shows the importance of buoyancy for urban flows, and eventually for the urban climate during heatwave events.

To qualitatively demonstrate how the coupled approach can provide a high spatial resolution and realistic urban flows, Fig. 8 shows the temperature and wind speed distributions above the ground (2 m and 10 m above the ground, respectively), generated by OpenFOAM and COSMO. The contours show hourly averaged values from 12-1 p.m., which is a hot hour period on both sample days. According to Fig. 8 (top left), the spatially and temporally varying lateral boundary conditions driven by COSMO can provide realistic wind maps within the city compared to assuming steady-state empirical inflow profiles at lateral boundaries.

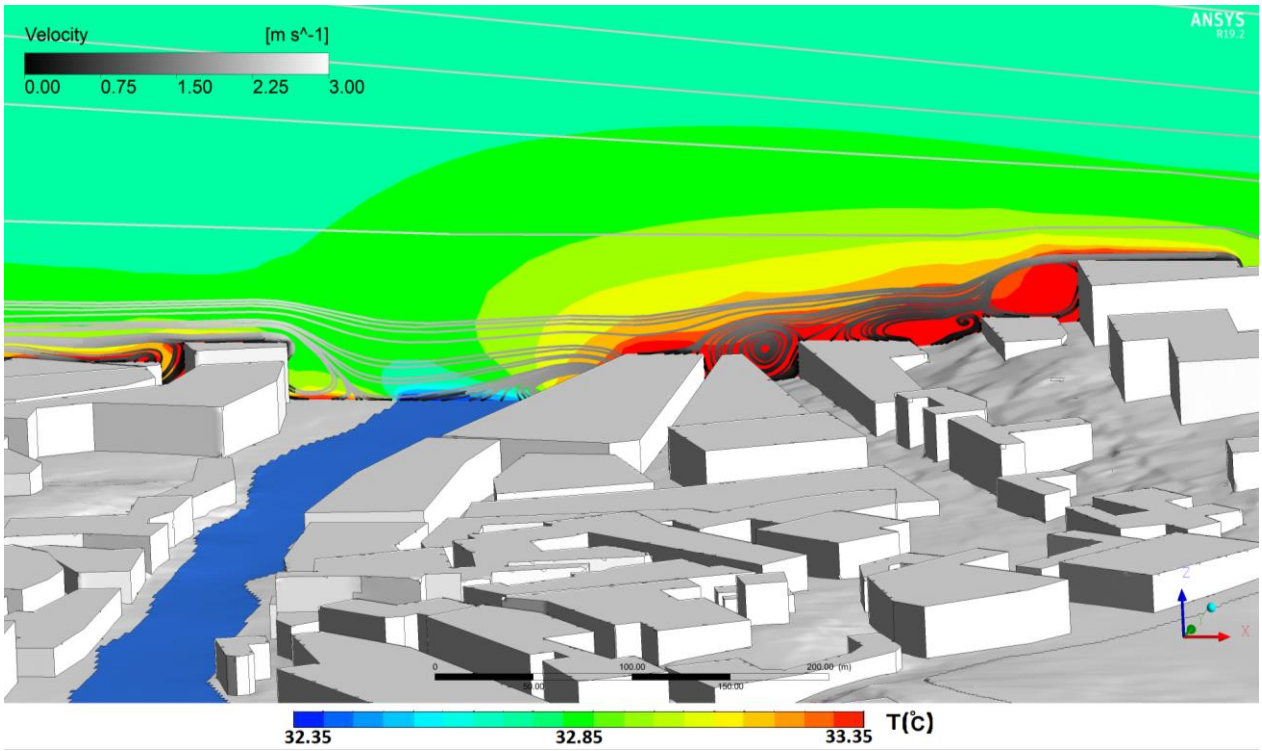

Fig 7. The upward and downward buoyant forces induced by the heated buildings and the river, respectively. The streamlines show how buoyancy can affect urban flows in the absence of strong synoptic winds during heatwaves. The streamlines and air temperatures are hourly averaged from 1-2 p.m on July 2.

From the vector field in the top left of Fig. 8, spatially irregular wind enters and leaves the domain from different parts of the lateral boundaries thanks to the dynamic coupling with COSMO. For example, a cold wind flows from the lake to the urban area, which could cool down the urban area adjacent to the north-west of the lake. In addition, a wind flow comes from the north and channelizes to the river path, which reaches the north-directed lake winds, results in a cool area at the west of the river. Comparing with the COSMO results shown on the right of Fig. 8, the coupled model provides a tool to study urban flows at finer scales. Wind and temperature patterns provided by COSMO cannot resolve the microscale wind patterns and merely show a north-directed wind, which cools down some parts of the urban area. The low resolution of COSMO cells and the inability of COSMO grid to include the steep changes of the orography, as well crude modeling of the effect of the urban morphology on the wind flow can be seen as the reasons for such a difference.

Figure 9 shows wind and temperature maps for June 23, 2015. Both COSMO and OpenFOAM show a strong east-directed wind. The wind speed reduces at the center of the domain due to the drag induced by the buildings and the transformation of mean mechanical energy into the turbulent kinetic energy. This results in wakes within the urban canopies. We can also see high wind speeds at the top left of the CFD domain, where a rail station is located (are not shown in the figures, but can be identified as a red spot in the OpenFOAM wind map at its top-left region), while in COSMO this high wind and low-temperature region could not be captured. Comparing the results for two days, the advantage of the coupled OpenFOAM model for simulation of urban flows, in comparison with using empirical profiles, is more pronounced for the heatwave day.

To highlight the temporal resolution obtained by dynamic coupling of COSMO with the URANS OpenFOAM model, the readers are referred to the supplementary animation of the article, which shows the diurnal development of the wind pattern in the urban area on July 2.

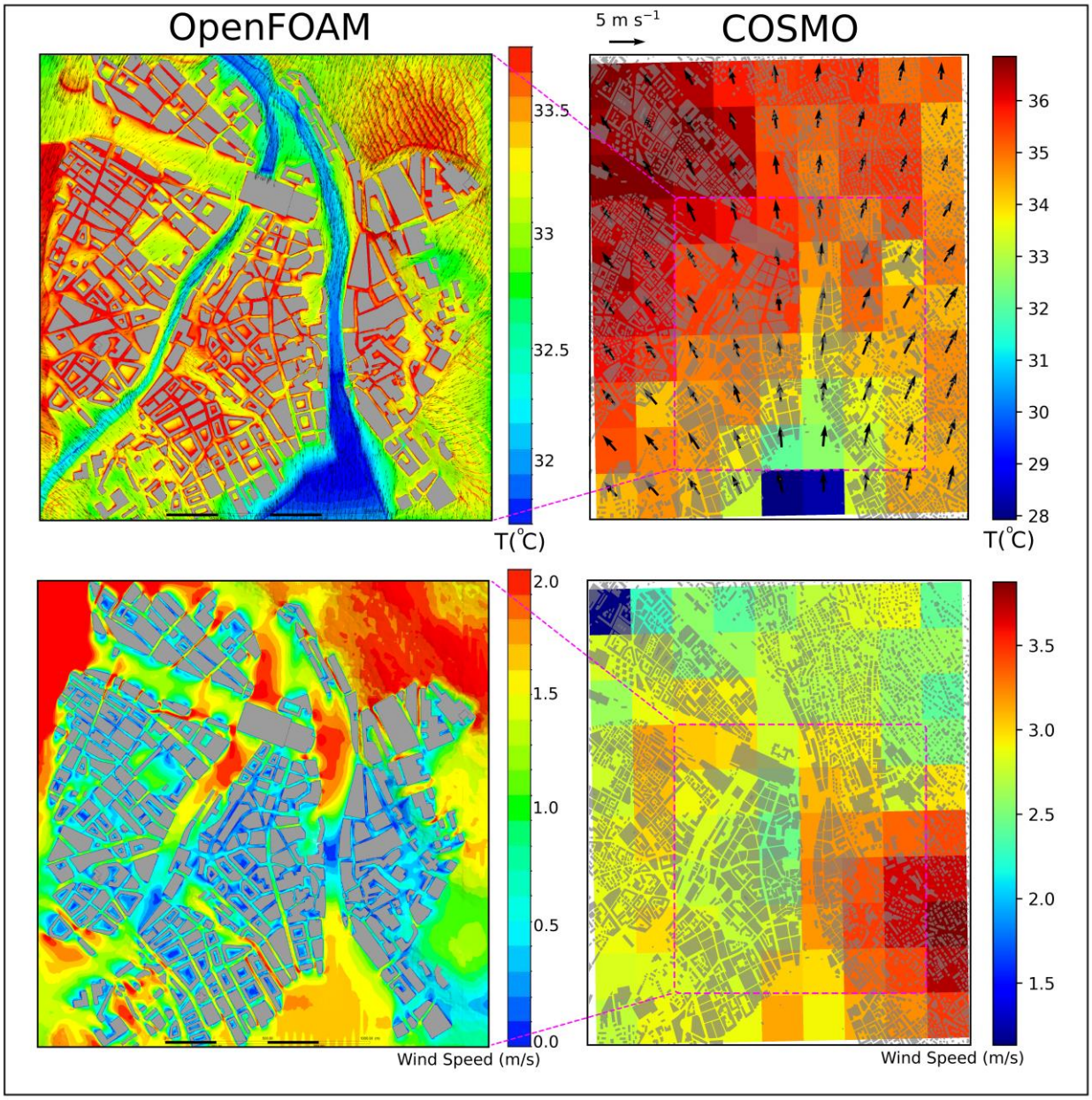

Fig. 8. The hourly averaged temperature and wind maps during the heatwave day of July 2, 2015, between 12 and 1 pm. Air temperatures and wind speeds are shown 2 m and 10 m above the ground, respectively. The top left map shows the temperature and wind vectors as computed by OpenFOAM, the top right is the counterpart computed by COSMO. The bottom left map shows the wind speed from OpenFOAM and the bottom map shows the wind by COSMO.

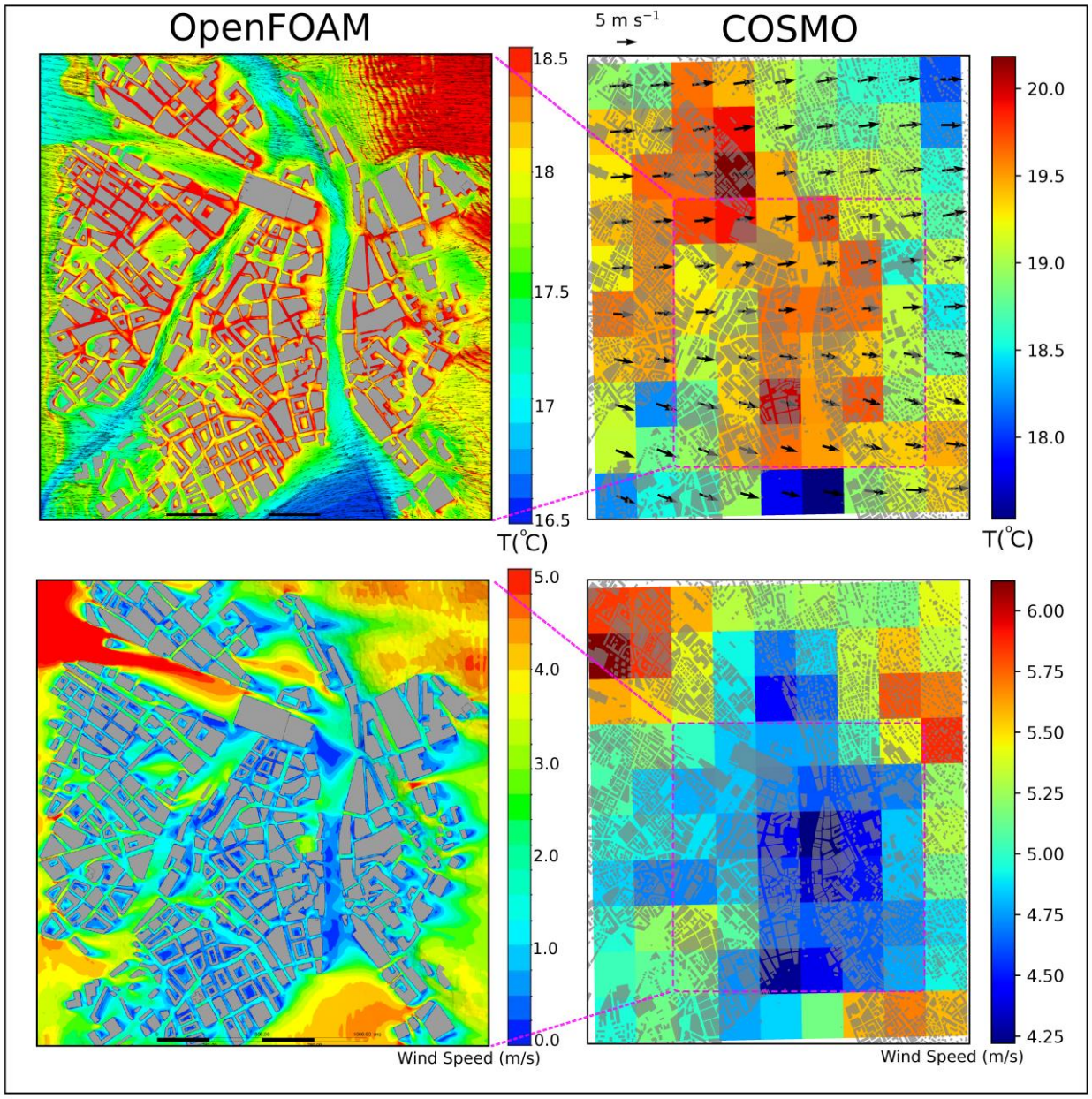

Fig. 9. The hourly average temperature and wind map on the typical summer day, June 23, 2015, at 12-1 pm. The air temperatures and the wind speeds are shown 2 m and 10 m above the ground, respectively. The top right contour is the temperature and wind vectors in OpenFOAM, the top left is the counterpart in COSMO. The bottom left contour is the wind speed map in OpenFOAM and the bottom right contour is the wind map by COSMO.

4-2- Preliminary quantitative assessment of the coupled approach

To evaluate the proposed coupling approach, the results of the OpenFOAM simulations are compared with the observations at the Zurich-Kaserne weather station and with the COSMO results. The Zurich-Kaserne site is located at the center-west of the domain (Fig. 10). Temperature is measured 2 m above the ground, at the coordinate (-467 m, 243 m) with respect to the center of the domain. Wind speed and the wind direction are measured 5 m above the roof (around 27 m above the ground) at the coordinate of (-446 m, 29 m) (Fig. 10). For COSMO, the temperatures at 2 m are diagnosed from the air temperature of the lowest mesoscale model layer and the average surface temperature (Schubert, 2013) [30]. The values at the exact location are interpolated from the closest corresponding COSMO cells.

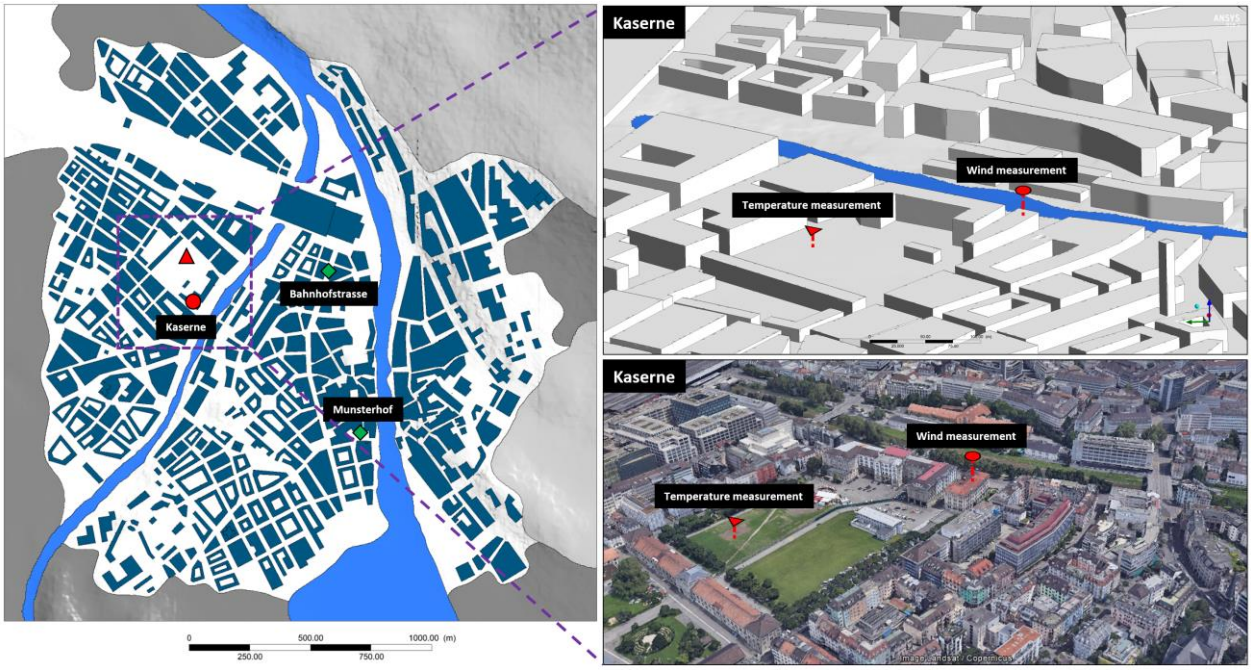

Fig. 10. Location of the observation points at Kaserne weather station (red signs) and two other sample locations for the mesh verification (orange signs on the left picture): Bahnhofstrasse and Munsterhof.

The comparisons are made for time series of the wind speed, wind direction and the temperature on June 23 (typical summer day) and July 2 (heatwave day), in a "forecast verification paradigm" (Wilks, 2011) [47]. The error scores used here are the bias (B), the root-mean-square error ($RMSE$), the unbiased root-mean-square error ($R\acute{M}SE$), and the Pearson correlation coefficient (r). As it was explained in section 3-3, due to storage limitation, results of OpenFOAM are saved every 50 seconds while for COSMO is every 15 or 30 minutes. To better compare the time series of simulations and the observation, the values of OpenFOAM and COSMO were averaged or linearly interpolated at 10 minutes observation intervals. Since the wind direction varies from -180 to 180 degree, to calculate the errors, if the difference between forecast and the observation ($\Delta\phi$) was higher than 180 degrees, the value was automatically corrected using the relation (Rodrigues et. al, 2016) [33]

$$\Delta\phi_{corrected} = \Delta\phi - 360\ \mathrm{sgn}(\Delta\phi)\ \max\big(0, \mathrm{sgn}(|\Delta\phi| - 180)\big). \tag{13}$$

First, the diurnal variation of the temperature forecasts on two sample days are depicted in Fig. 11. According to Fig. 11, the diurnal variation of the temperature on both sample days are well resolved by COSMO and accordingly by OpenFOAM. It can be seen for both sample days that COSMO slightly overpredicts around noon. OpenFOAM underpredicts on June 23 and calculates smoother daily profiles than observed on July 2. The bottom plots in Fig. 11 show diurnal variations of the root-mean-square error (RSME). The errors for both COSMO and OpenFOAM are in the same order during the days and for the most part below two degrees. The minimum errors for both models are found for the afternoon; perhaps because the atmospheric conditions are less variable. Highest errors are found for noon and between 20 p.m. to 4 a.m. The overall performance of the temperature forecasts can be assessed based on the score errors shown in Table 2. According to Table 2, for June 23 both COSMO and OpenFOAM predictions have high values of correlation (>0.9), meaning that they follow the observation trends. OpenFOAM has a positive mean error (overall overprediction), while COSMO's mean error is negative (overall underprediction). For both models, the order of RSME is almost the same, while their RSMEs are higher for July 2 compared to June 23. OpenFOAM's RSME for July 2 is 1.35, which is the greatest error. It can be concluded that for both models the accuracy of the calculated diurnal temperature variations at the reference location on the two sample days is in an acceptable range.

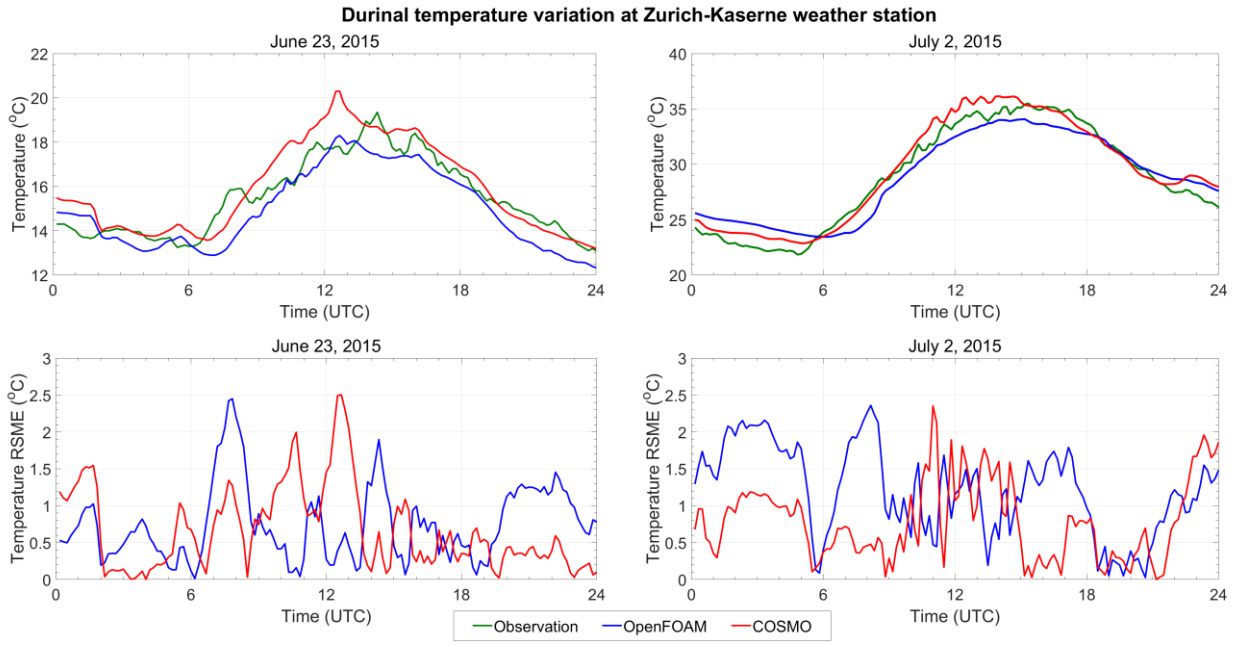

Fig. 11. Diurnal variations of temperature and RSME forecasts at Kaserne Station.

Fig. 12 shows the diurnal variation of the wind speed and associated RSME errors. On June 23, the OpenFOAM forecast generally follow the COSMO forecast and they could properly follow the observation time series with errors less than 1.5 m/s, except the overprediction from 5.m. to 8 a.m. and the underprediction from 11 a.m. to 12 p.m. The OpenFOAM errors in those periods are due to the errors coming from the COSMO-driven velocity boundary conditions, which mainly propagated from the west lateral boundary. OpenFOAM forecast mostly follows COSMO forecast since the winds are mostly caused by strong background regional winds resolved by COSMO rather than locally induced flows.

For July 2 COSMO overpredicts the wind speeds almost during the whole day and cannot properly follow the observed trend ($r = 0.2$). This overprediction may be due to the fact that COSMO parameterizes the effect of the buildings on the airflow by DCEP and cannot sense the aerodynamic effects of the building structures; e.g. the effect of the building (with 22 m height), on which the wind speed measurement device is mounted (5 m above its roof). This failure shows an inherent deficiency of the COSMO model in predicting local wind speeds at UCL and RSL. OpenFOAM follows the July 2 observation trend better with smaller errors ($r = 0.37$). The improved performance of OpenFOAM may be caused by the direct modeling of building and orography geometries and the higher spatial resolution of the surface temperatures.

As a general comparison of the forecasts between June 23, as a typical summer day, and July 2, as a heatwave day, the forecasts for June 23 have higher correlations than those for July 2 as shown in Fig. 12 and Table 2. Although the diurnal RSME variations in Fig. 12 and bias and RSME in Table 2 show higher errors for June 23, one should note that if we consider the debiased RḾSE (RSME subtracted by the systematic bias (the mean)), the errors for June 23 will be lower (this will be shown later in the Taylor diagram of Fig. 14). In addition, according to Table 2, an OpenFOAM RSME of 1.13 m/s and a COSMO RSME of 1.26 m/s for the diurnal range of 5-10 m/s wind speeds on June 23 are more acceptable than a RSME of 0.77 m/s and 1.20 m/s for the diurnal range of 1-3 m/s wind speeds on July 2. The lower forecasts performance for the wind speed on July 2 is understandable since during the heatwave the weak background regional and synoptic winds and the buoyant flows induced by high surface temperatures can be in the same order of magnitude and therefore compete with each other, which results in complex structures with varying wind speeds. This makes predictions difficult for both URANS based COSMO and OpenFOAM models.

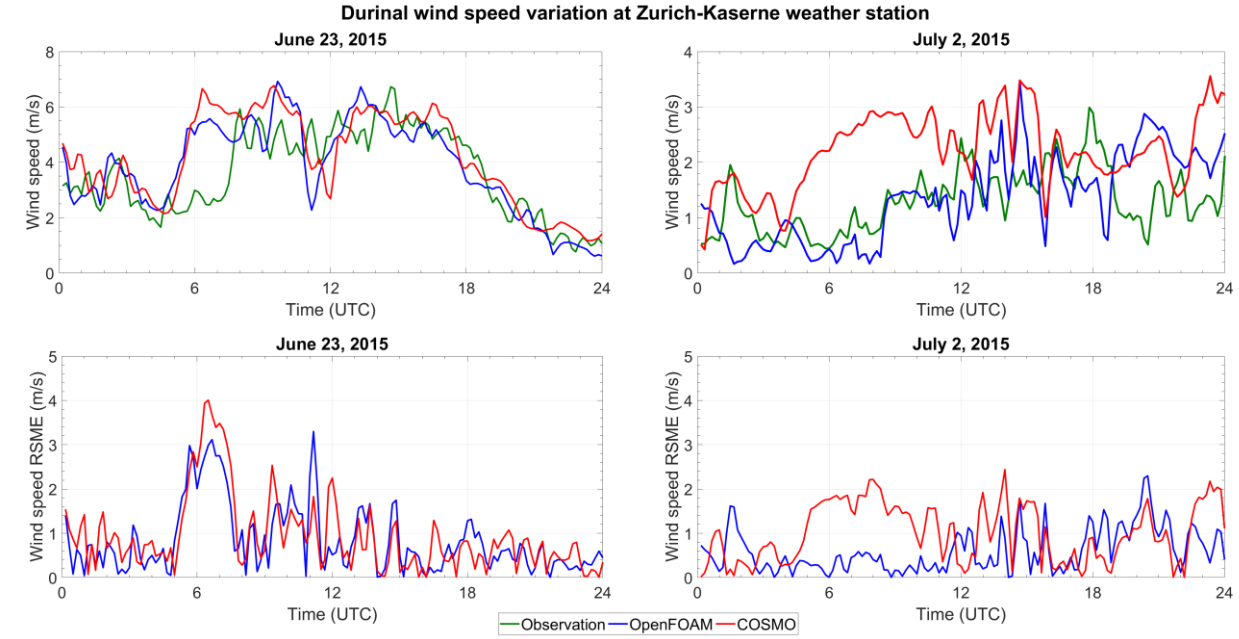

Fig. 12. Diurnal variations of wind speed and RSME forecasts at Kaserne Station.

The wind direction is another quantity of interest for urban microclimate studies. In particular, during weather conditions with moderate and high wind speeds, it is important to correctly predict the wind direction in order to get accurate predictions of the wind speeds and temperatures. Figure 13 shows the diurnal variations of the wind direction and the associated RSME. On June 23 the wind is dominantly flowing from west to east; probably due to a regional weather system with a persistent wind direction. The COSMO forecast, which is capable of capturing regional flows, follows the observation well. Since strong winds persistently flow from the western lateral OpenFOAM boundary into the domain, the OpenFOAM forecast is highly correlated to the COSMO forecast; note the diurnal RSME variations (left-bottom plot in Fig. 13). There is a high error period from 22 p.m. to 23 p.m. in the OpenFOAM results, which is mainly due to the errors from COSMO. Based on Table 2 both models follow to some degree the trend ($r = 0.35 - 0.4$); for both RSME is also around 40 degrees.

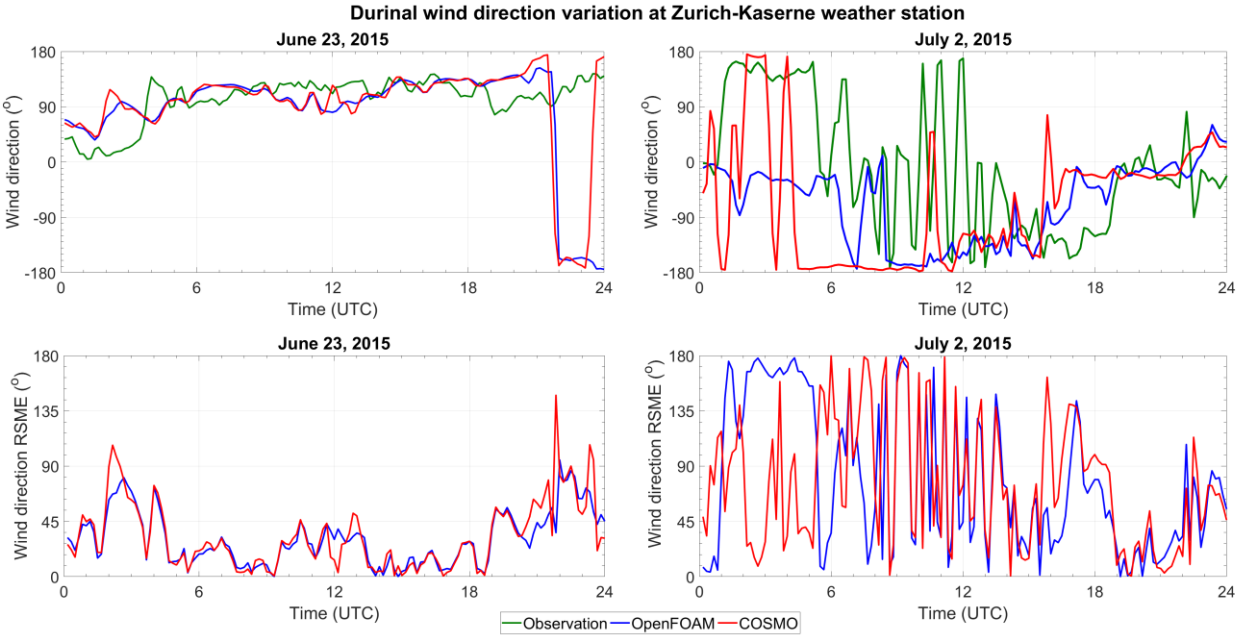

Fig. 13. Diurnal variations of wind direction and RSME forecasts at Kaserne Station.

The poorest forecasts performance are found in the predictions of wind direction during the heatwave day on July 2. The observations show a high variance in the wind direction and both COSMO and OpenFOAM fail to follow the trend. OpenFOAM's correlation is 0.18 and COSMO's correlation is even negative ($r = -0.20$), since it was unable to capture locally induced flows governed by local self-organized patterns. RSME for both forecasts is around 90-100 degree. It was somewhat expected that the meandering motion of the wind during the heatwave is difficult to predict, since the wind patterns are mainly caused by the combination of buoyancy and shear forces and dynamic instabilities. In the diurnal variations after 15 p.m., the errors reduce, which can be related to the easier prediction of wind direction with lower variance during that period. Generally, OpenFOAM error scores are lower for the wind direction during both sample days (same RSME, but better correlation), which can be related to direct modeling of building geometries.

Table 2. Forecast error scores

	Temperature						Wind Speed						Wind Direction					
	OpenFOAM			COSMO			OpenFOAM			COSMO			OpenFOAM			COSMO		
	B	*RMSE*	*r*	*B*	*RMSE*	*r*	*B*	*RMSE*	*r*	*B*	*RMSE*	*r*	*B*	*RMSE*	*r*	*B*	*RMSE*	*r*
June 23	-0.57	0.90	0.92	0.42	0.87	0.93	0.24	1.13	0.76	0.52	1.26	0.74	13.3	37.8	0.39	14.3	42.5	0.35
July 2	-0.08	1.35	0.97	0.49	0.95	0.98	0.05	0.77	0.37	0.91	1.20	0.20	-6.0	98.3	0.18	10.4	92.1	-0.20

To better illustrate the forecast performances and to compare them, we use a graphical tool named Taylor Diagram, which is frequently used in the atmospheric science community (Wilks, 2011) [47]. According to Fig. 14, a forecast is shown as a vertex. It creates a triangle in a polar coordinate system together with the observation vertex and the coordinate center. Based on the algebraic decomposition of the term "debiased mean square error $\acute{MSE}$" and the law of cosines, the lengths of two legs of the triangle will be the standard deviation of the observation SD_o and the standard deviation of the forecast SD_y (Wilks, 2011) [47]. The length of the third leg is the $\acute{RMSE}$. The angle between the vector from the center to the forecast vertex and the vector from the center to the observation vertex is the Pearson correlation r. For an easier comparison of temperature and wind speed forecasts, in the diagram of Fig. 14, we normalized all terms by SD_o, which allows us to superimpose their Taylor diagrams. The wind direction forecasts are not shown in the diagram, since the algebraic relation between SD_o, SD_y, $\acute{RMSE}$ and r may not hold true as Eq (13) is used to correct the calculated wind direction differences ($\Delta\phi$). Three main statistical forecast quantities are depicted in the diagram: The ratio of the standard deviations (SD_y/SD_o), which indicates the forecast variation magnitude compared to the observations, is shown by the radial distance from the origin (black dotted contour lines). The normalized unbiased (centered) root mean square error $\acute{RMSE}$, which shows the errors of the forecasts without considering the systematic (mean) errors, is shown by the distance from the observation vertex (green dashed contour lines). The correlation coefficient (r), which indicates the similarity in the patterns of the forecasts and the observations, is shown by the azimuth angle (blue dash-dotted contour lines). Eight red circles depicted in Fig. 14 show forecast temperatures and wind speeds by COSMO and OpenFOAM for the two sample days. It can be seen the best forecast (vertex closest to the observation vertex) is the temperature by COSMO on July 2 with the lowest $\acute{RMSE}$, highest correlation and the match of the standard deviation with that of the observations.

The worst forecasts are those of the wind speeds by OpenFOAM and COSMO on July 2. The OpenFOAM forecast variance is around 1.4 times that of the observation and for COSMO is 1.2. The COSMO results have a correlation with the observations of around 0.2 compared 0.37 for OpenFOAM. Both forecasts have almost the same $\acute{RMSE}$ error. Referring to Table 2, the COSMO wind speed forecasts RSME on July 2 is more related to the bias error, meaning that there is a systematic (mean) shift between COSMO and the observations.

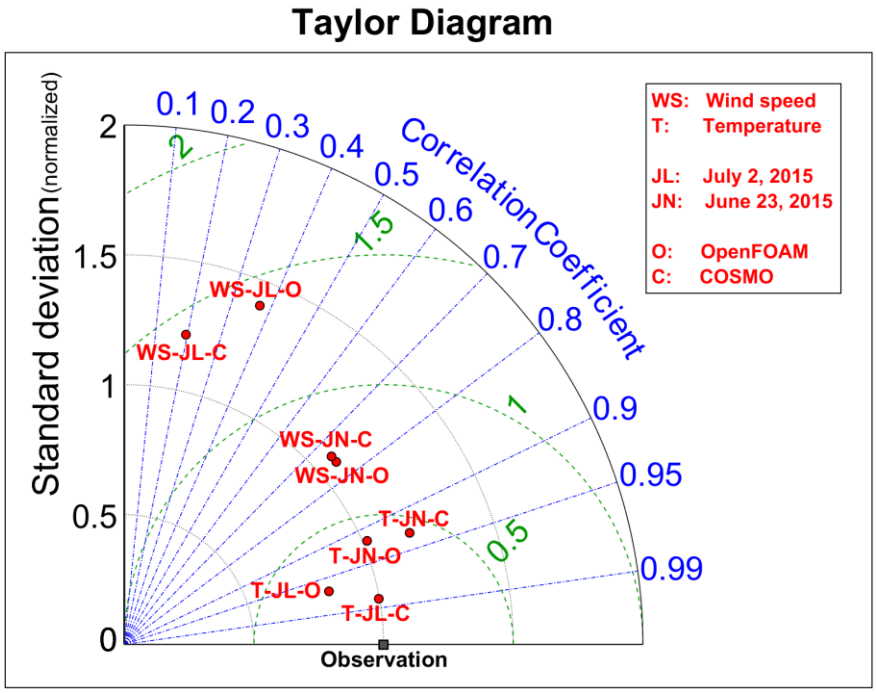

Fig. 14. Taylor diagram of temperature and wind speed forecasts. The ratio of the standard deviations (SD_y/SD_o) is shown by the radial distance from the origin (black dotted contour lines). The normalized unbiased (centered) root mean square error $RMSE$ is shown by the distance from the observation vertex (green dashed contour lines). The correlation coefficient (r) is shown by the azimuth angle (blue dash-dotted contour lines).

For the wind speed forecasts on June 23, COSMO and OpenFOAM forecasts are almost the same with slightly better performance for OpenFOAM (all correlations, standard deviation, and $RMSE$). Both COSMO and OpenFOAM provide better forecasts for June 23 in comparison to July 2, since the winds were stronger and more influenced by regional or synoptic flows than by local thermal flows. The slightly better wind speed predictions by OpenFOAM with respect to COSMO on both sample days can be attributed to the direct geometrical modeling of the buildings in OpenFOAM. However, due to the lack of enough measurement points and the complex nature of the wind field in the region, this conclusion should be taken with caution.

Comparing the temperature forecasts on the two sample days the COSMO forecasts on July 2 are better than on June 23 (of all three statistics). OpenFOAM performs better on July 2 compared to June 23 with respect to correlations and and $RMSE$, but not with respect to the standard deviation. In general, both models better predict the temperatures than wind speeds (In Fig. 14 closer to the observation vertex).

4-3- Discussion on the limitations of the coupled approach

The comparisons show that the proposed coupled approach is not fully capable of predicting the atmospheric quantities during the heatwave day. We diagnose the following important aspects for further improvement:

4-3-1- Microscale model

4-3-1-1- Transport model

The standard K-epsilon turbulence model used in this study has inherent limitations, e.g. linear eddy-viscosity assumption. In addition to a deficiency in predicting complex 3-D flows, such models cannot predict buoyant flows during heatwaves well, since they cannot consider anisotropy of the Reynolds stresses due to buoyancy. LES or higher moment RANS models with more sophisticated modeling of the effect of buoyancy can remedy this problem. As a trade-off in computational costs and accuracy, algebraic Reynolds stress and the turbulent heat flux models can be used where an additional transport equation for the

temperature variance can be solved (e.g. Hrebtov and Hanjalić, 2017) [48]. It should be noted, due to additional nonlinearities in the set of equations, using such models for complex urban geometries with low-quality mesh may lead to convergence difficulties.

The transport models also contain a number of free parameters which their values are not known for urban flows and may not be even constant. Calibration of such parameters for the urban flows can substantially improve the predictions. This can be done by parameter estimation techniques such as sequential or variational data assimilation.

The transport equations we solved were based on many simplistic assumptions which may deviate from a real urban boundary layer: incompressible flow, no Coriolis force, Bussinesque approximation for the buoyancy, a dry atmosphere, etc. Similar to the regional atmospheric models, full compressible flow, Coriolis force, and the moist atmosphere can be included into the CFD model, which can reduce the error of the predictions.

The airflow can be influenced by trees in urban canopy system and their effect should be included in the transport equations. The effect of trees can be modeled as sink or source terms in momentum, energy, turbulence, and moisture transport equations with e.g. porous medium concepts (e.g. Manickathan et. al, 2017) [49].

4-3-1-2- Surface fluxes:

While momentum fluxes at surfaces are rather easy to estimate (velocity is zero at the surface), heat fluxes (needed for estimation of buoyant fluxes) are highly dependent on surface temperatures. To attain higher accuracy, the values computed by DCEP with standard wall functions are not enough. Instead, SEB equations directly should be solved at surfaces considering the short-wave and long-wave radiative heat exchanges, the conduction in walls, and the sensible and the latent heat fluxes to the air (e.g. Kubilay et al., 2018) [15]. In such a case, to maintain high accuracies and low computational costs, the proposed coupled approach in this paper can be used as a driving model of a smaller nested domain where SEB is solved directly.

More accurate model to compute the fluxes to the air (e.g. to compute the sensible or latent heat flux in SEB from the surface temperature) is also very important. We used standard wall functions based on the equilibrium assumption which demands very thin wall cells heights. Generating such cells is very difficult for complex urban geometries and even so, it drastically increases the computational cost. If one uses coarse wall cells, then non-equilibrium effects, e.g. pressure gradient, convective fluxes, the buoyancy, etc. need to be included. Such non-equilibrium wall functions have been proposed by many researchers and should be used for urban flow applications (e.g. Popovac and Hanjalic, 2007, Allegrini et al., 2012) [35, 36].

4-3-2- Coupling method:

It was shown that the OpenFOAM model forecasts were highly correlated to COSMO forecasts, especially on the day with strong background winds. This suggests any possible errors from the mesoscale model can easily propagate into the microscale model. Therefore, to improve the predictions of the microscale model, the mesoscale model also needs improvement especially for difficult case studies such as heatwave days in a highly heterogeneous non-flat urban areas like the one we studied.

In addition, since two models use a different set of equations, even they are correct, they are still bounded to their simplification assumptions and the numerical errors can occur due to inconsistencies. Using the blending layer is a remedy for this issue, but one needs to make the models as close as possible to remove such errors. More advanced coupling strategy may also be helpful, e.g. two-way coupling strategies can be implemented and be optimized to reduce mismatches at the boundaries.

4-3-3- Computational aspects:

CFD simulation demands extensive computational resources and for practical applications, one should consider this aspect. In our study, we used URANS, which needs very small time steps to maintain convergence and physical results. Considering the mesoscale values were saved on large time steps, the timescale of changing of mean values from the lateral boundaries was so large that the time-derivative terms in OpenFOAM equations were not so large to influence the values of instantaneous state variables.

Therefore, to reduce the computational time, it may be better to use quasi-transient RANS at each time step of the mesoscale simulation.

The geometry resolution also highly affects the computational costs since it needs a larger mesh size. However, it has been shown by Ricci et al. (2017) [50] that increasing the geometrical resolution of buildings and other urban structures increases the accuracy. In our study, we used simplified LOD 1 and quite coarse mesh. To seek more accuracy higher LOD geometry models can be used at the expense of the computational costs.

4-3-4-Validation issue:

The question of whether the accuracy of the proposed coupled approach is enough remains unanswered. The comparisons between the two models and the observations (which was called a preliminary quantitative assessment) were based on one-point measurements. This means that the models' accuracy is just evaluated based on their capability to predict values at reference locations (2 m above a flat ground or 5 m above a building). This is not the full story since to study for example the urban microclimate, we need accurate 3-D temperature and wind speed data of the urban environment. On one hand, the success of both models in predicting temperatures (high correlations and small errors) do not necessarily guarantee the high accuracy of the computed temperature distributions within the urban environment. The errors can be very high at different locations like in the shaded area of a street canyon or close to roofs of tall buildings, especially since we did not directly model the radiation. On the other hand, the rather low improvement of OpenFOAM with respect to COSMO in wind speed and the wind direction predictions at the reference locations does not say so much about its general accuracy within the urban environment. Due to the higher resolution of the model, we can still expect OpenFOAM to provide results with less error COSMO inside the urban canyon layer, e.g. in the wake of buildings.
Therefore, to evaluate the coupled approach more comprehensively, we need a network of measurements in the neighborhood of the reference locations. Unfortunately, at the moment such a field measurement campaign has not been conducted yet. The available field measurements results are either based on distant individual towers or multiple close measurements but only close to the ground (no vertical profile). Using new technologies such as programmable drones may provide a useful dataset for validation of CFD urban microclimate models.

To evaluate and analysis of the microscale model performance and have generalizability of the conclusions, it is suggested that the coupled approach gets tested for a rather flat and large city, since the current case has heterogeneous city, lake, forests, and orography land use, which is very challenging for the models. In addition, the simulations should be performed for more and longer periods to better capture statistical quantities.

Lastly, one should acknowledge the urban flow is a complex system. Even if one can provide very accurate inputs for the CFD model, e.g. accurate transport and surface flux models, etc., due to the chaotic nature of the atmosphere and dynamical instabilities, the varying atmospheric state would be difficult to predict. In addition, both measurements and model parameters are uncertain and prone to errors. More advanced models have more parameters leading to more uncertainty in the results. Therefore, the CFD model results should be taken with care and if possible be accompanied by confidence intervals via e.g. uncertainty quantification approaches. In general, novel statistical approaches can be employed at the modeling and analysis levels to provide more credible and reliable CFD studies.

In spite of the limitations, considering the multi-scale nature of the urban atmosphere, we believe that the multi-scale coupled approach has a potential to at least improve the accuracy of the CFD microscale model by providing more accurate boundary conditions. In addition, without implementing any additional models, using DCEP for surface temperatures and COSMO for lateral boundary conditions, we can have computationally efficient simulations of urban flows with limited accuracy. The model can also be used for further nesting of more sophisticated models, e.g. with the model proposed by Kubilay et al. (2018) [15].

5- Conclusion

In this paper, we proposed a coupled approach for studying micro-atmospheric urban environment during heatwaves. A microscale CFD model was developed in OpenFOAM and was coupled with the regional atmospheric model COSMO and the urban canopy model DCEP in order to provide time-dependent boundary conditions. COSMO atmospheric variables were downscaled to the lateral and top boundaries of OpenFOAM and a blending layer was employed to reduce the numerical errors due to mismatches between the models. The time-dependent surface temperature of buildings and the ground was computed by solving surface energy balances in DCEP and was downscaled to OpenFOAM. The developed coupled model was tested for simulations of air flows in a dense urban area in Zurich, Switzerland. The simulations were performed for two sample days: one before starting a two-week heatwave event on June 23, 2015, as a typical summer day and one at the peak of the heatwave event on July 2, 2015.

It was shown that the coupled approach can provide high-resolution wind and temperature maps. For the heatwave day, the model could resolve buoyant flows induced by hot buildings and water bodies. Such small scale wind patterns could not be captured by COSMO since the model resolution is low and buildings effect is implicitly modeled. In addition, since the coupled approach uses a mesoscale model to resolve dynamical large scale weather phenomena, it has the potential to provide realistic results compared to CFD models with fitted empirical boundary conditions.

The quantitative comparison of the results with an observation measurement showed that generally, the accuracy of OpenFOAM forecasts depends on the COSMO performance. Especially on June 23, OpenFOAM diurnal time series followed the trend of COSMO time series, due to strong background regional winds resolved by COSMO. Different error scores revealed that the coupled OpenFOAM model managed to better forecast the atmospheric variables on June 23 compared to COSMO. However, both COSMO and OpenFOAM showed less accuracy in predicting wind speeds and directions for July 2, probably since the observed mean wind was highly fluctuating and was difficult to predict with the URANS model. It was shown OpenFOAM and COSMO temperature forecasts were quite accurate at the observation location.

The comparison with the one-point measurement should not be seen as validation. A comprehensive assessment with a well-located network of measurements is needed to assess the capability of the coupled approach in predicting wind and temperature 3-D distributions within UCL and RSL. We can conclude that further improvements in the models are still necessary in order to reach acceptable errors. In the transport model, the atmosphere model can be improved by considering the full compressible moist atmosphere. More advanced and calibrated RANS models or LES can improve the capability of simulating 3-D complex urban flows. Heat surface fluxes should be calculated by SEB equations modeling directly the radiation, conduction, and latent heat flux. The wall functions should also consider non-equilibrium effect especially if a coarse mesh is used. The higher resolution of the geometry can also increase accuracy. More consistency for mesoscale and microscale models may be needed and two-way coupling approach can improve the performance. There is plenty of room for further improvement in the model which can be addressed in future studies. Nonetheless, it is believed that the coupled approach can be a framework basis towards more reliable CFD models for studying urban flow and microclimate.

Acknowledgments

The authors would like to thank Prof. Patrick Jenny for his valuable comments and help in improving the manuscript. P. P., M. H. M., and E. A. would like to thank Mrs Nooshin Daneshpajooh and Professor Mohammad Arhami for their contribution in the development of software code and the methodology. P. P.

thanks Dominik Strebel for his technical support for the use of the HPC cluster. This work was supported by the ETH Research Grant ETH-08 16-2.

References

[1] Toparlar, Y., Blocken, B., Maiheu, B., & Van Heijst, G. J. F. (2017). A review on the CFD analysis of urban microclimate. *Renewable and Sustainable Energy Reviews*, *80*, 1613-1640.
[2] Mochida, A., Iizuka, S., Tominaga, Y., & Lun, I. Y. F. (2011). Up-scaling CWE models to include mesoscale meteorological influences. *Journal of Wind Engineering and Industrial Aerodynamics*, *99*(4), 187-198.
[3] Skamarock, W. C., Klemp, J. B., Dudhia, J., Gill, D. O., Barker, D. M., Wang, W., & Powers, J. G. (2005). *A description of the advanced research WRF version 2* (No. NCAR/TN-468+ STR). National Center For Atmospheric Research Boulder Co Mesoscale and Microscale Meteorology Div.
[4] Rockel, B., Will, A., & Hense, A. (2008). The regional climate model COSMO-CLM (CCLM). *Meteorologische Zeitschrift*, *17*(4), 347-348.
[5] Oke, T., Mills, G., Christen, A., & Voogt, J. (2017). Urban Climates. Cambridge: Cambridge University Press. doi:10.1017/9781139016476.
[6] Schättler, U., Doms, G., & Schraff, C. (2008). A description of the nonhydrostatic regional COSMO-model part VII: user's guide. *Tech. Rep., Deutscher Wetterdienst*.
[7] Lundquist, K. A., Chow, F. K., & Lundquist, J. K. (2010). An immersed boundary method for the weather research and forecasting model. *Monthly Weather Review*, *138*(3), 796-817.
[8] Li, D., & Bou-Zeid, E. (2013). Synergistic interactions between urban heat islands and heat waves: The impact in cities is larger than the sum of its parts. *Journal of Applied Meteorology and Climatology*, *52*(9), 2051-2064.
[9] Taleghani, M., Kleerekoper, L., Tenpierik, M., & van den Dobbelsteen, A. (2015). Outdoor thermal comfort within five different urban forms in the Netherlands. *Building and environment*, *83*, 65-78.
[10] Li, C., Zhou, S., Xiao, Y., Huang, Q., Li, L., & Chan, P. W. (2017, August). Effects of inflow conditions on mountainous/urban wind environment simulation. In Building Simulation (Vol. 10, No. 4, pp. 573-588). Tsinghua University Press.
[11] Richards, P. J., & Norris, S. E. (2011). Appropriate boundary conditions for computational wind engineering models revisited. *Journal of Wind Engineering and Industrial Aerodynamics*, *99*(4), 257-266.
[12] Temel, O., & van Beeck, J. (2017). Two-equation eddy viscosity models based on the Monin–Obukhov similarity theory. *Applied Mathematical Modelling*, *42*, 1-16.
[13] Schrijvers, P. J. C., Jonker, H. J. J., Kenjereš, S., & de Roode, S. R. (2015). Breakdown of the night time urban heat island energy budget. *Building and environment*, *83*, 50-64.
[14] Liu, Y. S., Miao, S. G., Zhang, C. L., Cui, G. X., & Zhang, Z. S. (2012). Study on micro-atmospheric environment by coupling large eddy simulation with mesoscale model. *Journal of Wind Engineering and Industrial Aerodynamics*, *107*, 106-117.
[15] Kubilay, A., Derome, D., & Carmeliet, J. (2018). Coupling of physical phenomena in urban microclimate: A model integrating air flow, wind-driven rain, radiation and transport in building materials. Urban climate, 24, 398-418.
[16] Jasak, H., Jemcov, A., & Tukovic, Z. (2007, September). OpenFOAM: A C++ library for complex physics simulations. In International workshop on coupled methods in numerical dynamics (Vol. 1000, pp. 1-20). IUC Dubrovnik, Croatia.
[17] Allegrini, J., & Carmeliet, J. (2018). Simulations of local heat islands in Zürich with coupled CFD and building energy models. Urban climate, 24, 340-359.
[18] Gao, Z., Bresson, R., Qu, Y., Milliez, M., de Munck, C., & Carissimo, B. (2018). High resolution unsteady RANS simulation of wind, thermal effects and pollution dispersion for studying urban renewal scenarios in a neighborhood of Toulouse. Urban Climate, 23, 114-130.
[19] Vonlanthen, M., Allegrini, J., & Carmeliet, J. (2017). Multiscale interaction between a cluster of buildings and the ABL developing over a real terrain. Urban Climate, 20, 1-19.
[20] Kwak, K. H., Baik, J. J., Ryu, Y. H., & Lee, S. H. (2015). Urban air quality simulation in a high-rise building area using a CFD model coupled with mesoscale meteorological and chemistry-transport models. Atmospheric Environment, 100, 167-177.
[21] Maronga, B., Gryschka, M., Heinze, R., Hoffmann, F., Kanani-Sühring, F., Keck, M., ... & Raasch, S. (2015). The Parallelized Large-Eddy Simulation Model (PALM) version 4.0 for atmospheric and oceanic flows: model formulation, recent developments, and future perspectives. *Geoscientific Model Development Discussions 8 (2015), Nr. 2, S. 1539-1637*.

[22] Martilli, A., Clappier, A., & Rotach, M. W. (2002). An urban surface exchange parameterisation for mesoscale models. *Boundary-layer meteorology*, *104*(2), 261-304.
[23] Schubert, S., Grossman-Clarke, S., & Martilli, A. (2012). A double-canyon radiation scheme for multi-layer urban canopy models. *Boundary-layer meteorology*, *145*(3), 439-468.
[24] Longo, R., Ferrarotti, M., Sánchez, C. G., Derudi, M., & Parente, A. (2017). Advanced turbulence models and boundary conditions for flows around different configurations of ground-mounted buildings. *Journal of wind engineering and industrial aerodynamics*, *167*, 160-182.
[25] Temel, O., Bricteux, L., & van Beeck, J. (2018). Coupled WRF-OpenFOAM study of wind flow over complex terrain. *Journal of Wind Engineering and Industrial Aerodynamics*, *174*, 152-169.
[26] Richards, P. J., & Norris, S. E. (2019). Appropriate boundary conditions for computational wind engineering: Still an issue after 25 years. *Journal of Wind Engineering and Industrial Aerodynamics*, *190*, 245-255.
[27] Henkes, R. A. W. M., Van Der Vlugt, F. F., & Hoogendoorn, C. J. (1991). Natural-convection flow in a square cavity calculated with low-Reynolds-number turbulence models. *International Journal of Heat and Mass Transfer*, *34*(2), 377-388.
[28] Doms, G., Schättler, U., & Baldauf, M. (2011). A Description of the Nonhydrostatic Regional COSMO model. Part I: Dynamics and Numerics. *Tech. rep., Deutscher Wetterdienst*.
[29] Doms, G., Förstner, J., Heise, E., Herzog, H. J., Mironov, D., Raschendorfer, M., ... & Vogel, G. (2011). A description of the nonhydrostatic regional COSMO model. Part II: physical parameterization. *Deutscher Wetterdienst, Offenbach, Germany*.
[30] Schubert, S. A. (2013). *Development and evaluation of a double-canyon urban canopy scheme, and estimation of urban heat island mitigation effects* (Doctoral dissertation, Freie Universität Berlin Berlin).
[31] Haji Mohammadi, M., Sotiropoulos, F., & Brinkerhoff, J. (2019). Moving least squares reconstruction for sharp interface immersed boundary methods. *International Journal for Numerical Methods in Fluids*, *90*(2), 57-80.
[32] Tewari, M., Kusaka, H., Chen, F., Coirier, W. J., Kim, S., Wyszogrodzki, A. A., & Warner, T. T. (2010). Impact of coupling a microscale computational fluid dynamics model with a mesoscale model on urban scale contaminant transport and dispersion. *Atmospheric Research*, *96*(4), 656-664.
[33] Rodrigues, C. V., Palma, J. M. L. M., & Rodrigues, Á. H. (2016). Atmospheric flow over a mountainous region by a one-way coupled approach based on Reynolds-averaged turbulence modelling. *Boundary-layer meteorology*, *159*(2), 407-437.
[34] Blocken, B., Stathopoulos, T., & Carmeliet, J. (2007). CFD simulation of the atmospheric boundary layer: wall function problems. *Atmospheric environment*, *41*(2), 238-252.
[35] Popovac, M., & Hanjalic, K. (2007). Compound wall treatment for RANS computation of complex turbulent flows and heat transfer. *Flow, turbulence and combustion*, *78*(2), 177.
[36] Allegrini, J., Dorer, V., Defraeye, T., & Carmeliet, J. (2012). An adaptive temperature wall function for mixed convective flows at exterior surfaces of buildings in street canyons. *Building and Environment*, *49*, 55-66.
[37] Amt für Städtebau. (2019, May 03). Retrieved from https://www.stadt-zuerich.ch/hbd/de/index/staedtebau/afs.html
[38] Gröger, G., Kolbe, T. H., Czerwinski, A., & Nagel, C. (2008). OpenGIS city geography markup language (CityGML) implementation specification. *Version*, *1*(0), 08-007.
[39] Koblitz, T., Bechmann, A., Sogachev, A., Sørensen, N., & Réthoré, P. E. (2015). Computational Fluid Dynamics model of stratified atmospheric boundary- layer flow. *Wind Energy*, *18*(1), 75-89.
[40] Mellor, G. L., & Yamada, T. (1982). Development of a Turbulence Closure Model for Geophysical Fluid Problems. Reviews of Geophysics and Space Physics, 20(4), 851–875.
[41] Ritter, B., & Geleyn, J. F. (1992). A comprehensive radiation scheme for numerical weather prediction models with potential applications in climate simulations. Monthly Weather Review, 120(2), 303-325.
[42] Tiedtke, M. I. C. H. A. E. L. (1989). A comprehensive mass flux scheme for cumulus parameterization in large-scale models. Monthly Weather Review, 117(8), 1779-1800.
[43] Mussetti, G. , Brunner, D. , Allegrini, J. , Wicki, A. , Schubert, S. and Carmeliet, J. (2019), Simulating urban climate at sub- kilometre scale for representing the intra- urban variability of Zurich, Switzerland. Int J Climatol. (In-press) doi:10.1002/joc.6221
[44] Schraff, C. H. (1997). Mesoscale data assimilation and prediction of low stratus in the Alpine region. Meteorology and Atmospheric Physics, 64(1–2), 21–50.
[45] Swisstopo. 2010. swissBUILDINGS3D 1.0.
[46] Loridan, T., & Grimmond, C. S. B. (2012). Multi- site evaluation of an urban land- surface model: intra- urban heterogeneity, seasonality and parameter complexity requirements. Quarterly Journal of the Royal Meteorological Society, 138(665), 1094-1113.

[47] Wilks, D. S. (2011). *Statistical methods in the atmospheric sciences* (3rd ed.). Oxford; Waltham, MA: Academic Press.
[48] Hrebtov, M., & Hanjalić, K. (2017). Numerical study of winter diurnal convection over the city of Krasnoyarsk: Effects of non-freezing river, undulating fog and steam devils. Boundary-Layer Meteorology, 163(3), 469-495.
[49] Manickathan, L., Defraeye, T., Allegrini, J., Derome, D., & Carmeliet, J. (2018). Parametric study of the influence of environmental factors and tree properties on the transpirative cooling effect of trees. Agricultural and Forest Meteorology, 248, 259-274.
[50] Ricci, A., Kalkman, I., Blocken, B., Burlando, M., Freda, A., & Repetto, M. P. (2017). Local-scale forcing effects on wind flows in an urban environment: Impact of geometrical simplifications. Journal of Wind Engineering and Industrial Aerodynamics, 170, 238-255.